Evaluating a fire smoke simulation algorithm in the National Air Quality Forecast Capability (NAQFC) by using multiple observation data sets during the Southeast Nexus (SENEX) field campaign

Li Pan [1,2*], HyunCheol Kim [1,2], Pius Lee [1], Rick Saylor [3], YouHua Tang [1,2], Daniel Tong [1,4], Barry Baker [1,5], Shobha Kondragunta [6], Chuanyu Xu [7], Mark G. Ruminski [6], Weiwei Chen [9], Jeff Mcqueen [10] and Ivanka Stajner [10]

[1] NOAA/OAR/Air Resources Laboratory, College Park, MD 20740, USA

[2] UMD/Cooperative Institute for Satellite Earth System Studies (CISESS), College Park, MD 20740, USA

[3] NOAA/OAR/ARL/Atmospheric Turbulence and Diffusion Division, Oak Ridge, TN 37830, USA

[4] GMU/CISESS, Fairfax, VA 22030, USA

[5] UMBC/CISESS, Baltimore, MD 21250, USA

[6] NOAA/NESDIS, College Park, MD 20740, USA

[7] I. M. Systems Group at NOAA, College Park, MD 20740, USA

[9] Northeast Institutes of Geography and Agroecology, Chinese Academy of Sciences, Changchun 130102, P. R. China

[10] NOAA/NCEP/Environmental Modeling Center, College Park, MD 20740, USA

Correspondence to: Li.Pan@noaa.gov

*Now at: *[NOAA/NCEP/EMC and I.M.S.G]*

Abstract

Multiple observation data sets: Interagency Monitoring of Protected Visual Environments (IMPROVE) network data, Automated Smoke Detection and Tracking Algorithm (ASDTA), Hazard Mapping System (HMS) smoke plume shapefiles and aircraft acetonitrile (CH_3CN) measurements from the NOAA Southeast Nexus (SENEX) field campaign are used to evaluate the HMS-BlueSky-SMOKE-CMAQ fire emissions and smoke plume prediction system. A similar configuration is used in the US National Air Quality Forecasting Capability (NAQFC). The system was found to capture most of the observed fire signals. Usage of HMS-detected fire hotspots and smoke plume information were valuable for both deriving fire emissions and forecast evaluation. This study also identified that the operational NAQFC did not include fire contributions through lateral boundary conditions resulting in significant simulation uncertainties. In this study we focused both on system evaluation and evaluation methods. We discussed how to use observational data correctly to retrieve fire signals and synergistically use multiple data sets. We also addressed the limitations of each of the observation data sets and evaluation methods.

Introduction

Wildfires and agricultural/prescribed burns are common in North America all year round, but predominantly occur during the spring and summer months (Wiedinmyer et al., 2006). These fires pose a significant risk to air quality and human health (Delfino et al., 2009; Rappold et al., 2011; Dreessen et al., 2016; Wotawa and Trainer 2000; Sapkota et al., 2005; Jaffe et al., 2013; Johnston et al., 2012). Since January 2015, smoke emissions from fires have been included in the National Air Quality Forecasting Capability (NAQFC) daily $PM_{2.5}$ operational forecast (Lee et al., 2017). The NAQFC fire simulation consists of: the NOAA National Environmental and Satellite Data and Information Service (NESDIS) Hazard Mapping System (HMS) fire detection algorithm, the U.S. Forest Service (USFS) BlueSky-fire emissions

estimation algorithm, the U.S. EPA Sparse Matrix operator Kernel Emission (SMOKE) applied for fire plume rise calculations, the NOAA National Weather Service (NWS) North American Multi-scale Model (NAM) for meteorological prediction and the U.S. EPA Community Multi-scale Air Quality Model (CMAQ) for chemical transport and transformation. In contrast to most anthropogenic emissions, smoke emissions from fires are largely uncontrolled, transient and unpredictable. Consequently, it is a challenge for air quality forecasting systems such as NAQFC to describe fire emissions and their impact on air quality (Pavlovic et al., 2016; Lee et al., 2017; Huang et al., 2017).

Southeast Nexus (SENEX) was a NOAA field study conducted in the Southeast U.S. in June and July 2013 (Warneke et al., 2016). This field experiment investigated the interactions between natural and anthropogenic emissions and their impact on air quality and climate change (Xu et al., 2016; Neuman et al., 2016). In this work, the SENEX dataset was used to evaluate the HMS-BlueSky-SMOKE-CMAQ fire simulations during the campaign period.

Two simulations were performed: one with and one without smoke emissions from fires during the SENEX field campaign. Due to the large uncertainties in the estimates of fire emissions and smoke simulations (Baker et al., 2016; Davis et al., 2015; Drury et al., 2014), the first step of the evaluation focused on the fire signal capturing capability of the system. Differences between the two simulations represented the impact of the smoke emissions from fires on the CMAQ model results. Observations from various sources were utilized in this analysis: (i) ground observations (Interagency Monitoring of Protected Visual Environments (IMPROVE)), (ii) satellite retrievals (Automated Smoke Detection and Tracking Algorithm (ASDTA) and HMS smoke plume shape), and (iii) aircraft measurements (SENEX campaign). Fire signals predicted by the modeling system were directly compared to these observations. Several criteria have been used to rank efficacy of the observation systems for fire induced pollution plumes.

Methodology

In this section the NAQFC fire modeling system used in the study was introduced. Uncertainties and limitations in the various modeling components of the system are discussed. Fig. 1 illustrates the schematics of the system. There are four processing steps:

HMS (Hazard Mapping System)

The NOAA NESDIS HMS is a fire smoke detection system based on satellite retrievals. At the time of this study, the satellite constellation used consists of 2 Geostationary Operational Environmental Satellite (GOES-10 and GOES-12) and 5 polar orbiting satellites: MODIS (Moderate-resolution Imaging Spectroradiometer)) instruments on NASA EOS -- Terra and Aqua satellites, and AVHRR (Advanced Very High Resolution Radiometer) instruments on NOAA 15/17/18 satellites. HMS detects wildland fire locations and analyzes their sizes, starting times and durations (Ruminski et al., 2008; Schroeder et al., 2008; Ruminski and Kondragunta 2006).

HMS first processes satellite data by using automated algorithms for each of the satellite platforms to detect fire locations (Justice et al., 2002; Giglio et al., 2003; Prins and Menzel 1992; Li et al., 2000), which is then manually analyzed by analysts to eliminate false detections and/or add missed fire hotspots. The size of the fire is represented by the number of detecting pixels corresponding to the nominal resolution of MODIS or AVHRR data. Fire starting times and durations are estimated from close inspection of the visible band satellite imagery. A bookkeeping file is generated at the end of this detection step, named “hms.txt” (Fig. 1). It includes all the thermal signal hotspots detected by the aforementioned 7 satellites. During the analyst quality control step, detected potential fire hotspots lacking visible smoke in the retrieval’s HMS (RGB real-color) imagery are removed resulting in a reduced fire hotspot file called either “hmshysplit.prelim.txt” or “hmshysplit.txt” to be input into the BlueSky processing step.

In general, “hmshysplit.prelim.txt” and “hmshysplit.txt” are very similar, and “hmshysplit.txt” is created later than “hmshysplit.prelim.txt” (Fig. 1). But the differences between “hmx.txt” and “hmshysplit.txt” (“hmshysplit.prelim.txt”) can be rather substantial. The reasons for differences are: 1) many detected fires do not produce detectable smoke; 2) some fires/hotspots are detected only at night, when smoke detection is not possible; 3) smoke emission HMS imagery is obscured by clouds thus not detected by the analyst. Therefore, smoke emission occurrence provided by the HMS is a conservative estimate of fire emissions.

By using multiple satellites the likelihood of detecting fires in HMS is robust. However, when the fire geographical size is small the HMS detection accuracy dramatically decreases (Zhang et al., 2011; Hu et al., 2016). Other limitations of the HMS fire detections include ineffective retrievals at nighttime and under cloud cover.

BlueSky

BlueSky, developed by the USFS (US Forest Service), is a modeling framework to simulate smoke impacts on regional air quality (Larkin et al., 2009; Strand et al., 2012). In this study, BlueSky acted as a fire emission model to provide input for SMOKE (Herron-Thorpe et al., 2014; Baker et al., 2016). BlueSky calculates fire emission based on HMS-derived locations (Fig. 1).

Fire geographical extent is reflected by the number of nearby fire pixels detected by satellites in a 12-km CMAQ model grid. Fire pixels are converted to fire burning areas in BlueSky based on the assumption that each fire pixel has a size of 1 km^2 and 10% of its area can be considered as burn-active (Rolph et al., 2009). All fire pixels in a 12-km grid square are aggregated. BlueSky uses the following to estimate biomass availability: fuel loading map is from the US National Fire Danger Rating System (NFDRS) for the Conterminous US (CONUS) with the exception in western US where the HARDY set is used (Hardy and Hardy 2007). BlueSky uses Emissions Production Model (EPM) (Sandberg and Peterson

1984), a simple version of CONSUME, to calculate fuel actually burned -- the so-called consumption sums. Finally, EPM is also used in BlueSky to calculate the fire emission hourly rate per grid-cell. BlueSky outputs CO, CO_2, CH_4, non-methane hydrocarbons (NMHC), total PM, $PM_{2.5}$, PM_{10} and heat flux (Fig. 1).

BlueSky does not iteratively recalculate fire duration according to the modeled diminishing fuel loading or the modeled fire behavior. In the aggregation process, when there is more than one HMS point in a grid cell which have different durations, all points in that grid cell would be assigned the largest duration in all points. For an example, if there were 3 HMS points that had durations of 10, 10 and 24 hours, the aggregation would include 3 points (representing 3 km^2) assigned with 24 hour duration to all of the 3 HMS points.

HMS has no information about fuel loading. BlueSky uses a default fuel loading climatology over the eastern US. BlueSky uses an idealized diurnal profile for fire emissions. Uncertainties in fire sizes, fuel loading and fire emission rates lead to large uncertainties in wildland smoke emissions (Knorr et al., 2012; Drury et al., 2014; Davis et al., 2015).

SMOKE

In SMOKE (Sparse Matrix Operator Kernel Emission), the BlueSky fire emissions data in a longitude-latitude map projection are converted to CMAQ ready gridded emission files (Fig. 1). Fire smoke plume rise is calculated using formulas by Briggs. The heat flux from BlueSky and NAM meteorological state variables are used as input (Erbrink 1994). The Briggs' algorithm calculates plume top and plume bottom, between plume top and bottom the emission fraction is calculated layer by layer assuming a linear distribution of flux strength in atmospheric pressure. For model layers below the plume bottom the emission fraction is assumed to be entirely in the smoldering condition as a function of the fire burning area.

A speciation cross-reference map was adopted to match BlueSky chemical species to that in CMAQ using the U.S. EPA Source Classification Codes (SCCs) for forest Wildfires (https://ofmpub.epa.gov/sccsearch/docs/SCC-IntroToSCCs.pdf). The life-span of fire is based on the HMS detected fire starting time and duration. During fire burning hours a constant emission rate is assumed. This constant burn-rate has been shown to be a crude estimate (Saide et al., 2015; Alvarado et al., 2015). Other uncertainties include plume rise (Sofiev et al., 2012; Urbanski et al., 2014; Achtemeier et al., 2011) and fire-weather (fire influencing local weather).

CMAQ

The CMAQ version 4.7.1 was used. The CB05 gas phase chemical mechanism (Yarwood et al., 2005) and the AERO5 aerosol module (Carlton et al., 2010) were chosen. Anthropogenic emissions were based on the U.S. EPA 2005 National Emission Inventory (NEI) projected to 2013 (Pan et al., 2014), Biogenic emissions (BEIS 3.14) were calculated in-line inside CMAQ.

Simulations

The NAM provided meteorology fields to drive CMAQ (Chai et al., 2013). NAM meteorology is evaluated daily and results (BIAS and RMSE etc.) are posted on: "http://www.emc.ncep.noaa.gov/mmb/mmbpll/mmbverif/". The simulation domain is shown in Fig. 1. It includes two domains: (i) a 12-km domain covering the Continental U.S. (CONUS); and (ii) a 4km domain covering the Southeast U. S. where the majority of SENEX measurements occurred. Lateral boundary conditions (LBC) used in the smaller SENEX domain simulation were extracted from that from the CONUS simulations. Four scenarios were simulated: CONUS with fire emissions, CONUS without fire emissions, SENEX with fire emissions and SENEX without fire emissions.

There were several differences in system configuration between the NAQFC fire smoke forecasting and the "with-fire" simulation in this study. For models, the BlueSky versions used in NAQFC

and that in this study are v3.5.1 and v2.5, respectively; CMAQ versions used in NAQFC and in this study are v5.0.2 and v4.7.1, respectively. For simulations, current fire smoke forecasting in the NAQFC includes two runs: the analysis and the forecast (Huang et al. 2019 (manuscript in preparation)). The analytical run is a 24-hour retrospective simulation using yesterday's meteorology and fire emissions to provide initial conditions for today's forecast. The forecasting run is a 48-hour predictive simulation using yesterday's fire emissions, assuming fires with duration of more than 24 hours are projected as continued fires.. The "with-fire" simulation in this study is exactly identical to the analysis run in NAQFC.

Evaluations

Carbon monoxide (CO) has a relatively long life time in the air and is emitted by biomass burning. CO was used as a fire tracer in the prediction. The CO difference (ΔCO) between CMAQ simulations with and without fire emissions was used as the indicator of fire influence. For additional observations included: potassium (K) collected at the IMPROVE (Interagency Monitoring of Protected Visual Environments) sites within the SENEX domain; acetonitrile (CH_3CN) measured from the SENEX campaign flights; and fire plume shape detected by the HMS analysis as real fire signals. The enhancement in ΔCO concentration due to fire was directly compared with those signals. At the same time, ΔAOD (Aerosol Optical Depth) from CMAQ ("with-fire" simulated concentration minus that with "without-fire") was also used as fire indicator when compared with smoke masks given by the ASDTA (Automated Smoke Detection and Tracking Algorithm).

It is almost impossible to assess the uncertainty of each specific smoke physical process. In each modeling step in HMS, BlueSky, SMOKE and CMAQ, the modeling system accrues uncertainties. Such uncertainties were likely cumulative and might lead to larger error in succeeding components (Wiedinmyer et al., 2011). For an example, heat flux from BlueSky influenced plume rise height in SMOKE and consequently influenced plume transport in CMAQ. It is also noteworthy that when

modeled ΔCO was against measured K or CH_3CN, the objective was to search for enhancement signals resulting from fires but not aiming to account for proportional concentration changes in the tracers in the event of a fire. Attempting to account for CMAQ simulation uncertainties in surface ozone and particulate matter as a function of smoke emissions from fires was difficult. Neither was it the objective of this study. Rather, the purpose of this study is to focus on analyzing the capability of the HMS-BlueSky-SMOKE-CMAQ modeling system to capture fire signals.

The SENEX campaign occurred in June and July and our model simulations were from June 10 to July 20, 2013. Throughout the campaign all available observation datasets were used including ground-, air- and satellite-based acquired data. Each dataset had its unique characteristics and linking them together gave an overall evaluation. At the same time, in each dataset our evaluations included as many as possible observed fire cases. Both well-predicted and poorly-predicted cases are presented to illustrate potential reasons responsible for the modeling system's behavior.

Results and Discussions

Observed CO versus modeled CO in SENEX

Table 1 lists observed and modeled CO vertical profiles for the "with-fire" and "without-fire" cases during the SENEX campaign. Observed CO concentrations between the surface and 7 km AGL (Altitude above Ground Level) in the SENEX domain area remained greater than 100 ppb during all 40 days of the campaign. The highest CO concentrations were measured closer to the surface. The maximum measured CO concentration of 1277 ppb was observed during a flight on July 03 at an ASL (Altitude above Sea Level) of 974 m. In this flight strong fire signals were observed but the fire simulation system missed those signals as discussed below.

CO concentrations were underestimated by the model in almost all cases even when the model captured CO contribution from fire emissions spatio-temporarily. Mean ΔCO in each height interval was usually above 1.5 ppb but less than 2.0 ppb. Fig. 2a shows the contribution of total CO emissions from fires which occurred inside the SENEX domain over the simulation period. The maximum CO emissions contribution from fires was about 3% during the campaign. In most of those days fire emission contributions in SENEX were less than 1%. The averaged contribution during those 40 days was 0.7%. Fig. 2b shows the contribution of CO flowing into the SENEX domain from its boundary caused by fire outside the SENEX domain but inside the CONUS domain (Fig. 1). The averaged fire contribution to CO from outside the SENEX domain was 0.67%. CO influenced by fire emission in June is greater than that in July.

During the field experiment the general lack of large fires made evaluation of modeled fire signature difficult since it was easier to capture large fire signals than the smaller fires. We postulated that a clear fire signal simulated in the HMS-BlueSky-SMOKE-CMAQ system could be indicated by ΔCO significantly larger than its temporal averages resulted by fires originated from inside and/or outside the SENEX domain. For an example, a clear fire signal between 500 m and 1000 m AGL was indicated by ΔCO across those altitudes and when the concentration of ΔCO was above 2.0 ppb based on the campaign duration averaged CO concentration of about 150 ppb as well as on within the SENEX domain and outside of the SENEX domain fire contributions to CO (150*(0.007+0.0067) =2.0).

Figure 3 displays the simulated ΔCO extracted along SENEX flight path during the SENEX campaign. The modeled concentration showed that the fire impacts on SENEX were not negligible despite a lack of larger fire events as shown in Fig. 2a and 2b during the SENEX campaign period. That confirmed the importance of evaluating the fire simulation system in an air quality model. Unless a model is able to predict fire signals correctly it is useless for modelers to discuss fire effects on chemical

composition of the atmosphere. A detail of how model caught or missed or falsely predicted fire signals during the SENEX campaign and a comparison of ΔCO versus CH_3CN will be discussed in the follow discussion.

IMPROVE

The Interagency Monitoring of Protected Visual Environments (IMPROVE) is a long term air visibility monitoring program initiated in 1985 (http://vista.cira.colostate.edu/Improve/data-page). It provides 24-h integrated particulate matter (PM) speciation measurements every third day (Malm et al., 2004; Eatough et al., 1996). The IMPROVE dataset was chosen for this analysis because it included K (potassium), OC (organic carbon) and EC (elemental carbon), important fire tracers. IMPROVE monitors are ground observation sites likely influenced by nearby fire sources.

There were 14 IMPROVE sites in the SENEX domain (Fig. 4). Potential fire signals were identified by using CMAQ modeled ΔCO and IMPROVE observed K. However, in addition to fires K has multiple sources such as soil, sea salt and industry. Co-incidentally fires should also produce enhanced EC and OC concentrations, a fire signal should reflect above-average values for EC, OC, and K. EC, OC and K observations that were 20% above their temporal averages during the SENEX campaign were used as a predictor for fire event identification. Meanwhile, co-measured NO_3^- and SO_4^{2-} concentrations are less than 1.5 times of their respective temporal averages for screening out data with industrial influences. Lastly, a third predictor was employed so that concentrations of other soil components besides K should be below their temporal average to eliminate conditions of spikes in K concentration due to dust. With these three criteria the IMPROVE data was screened for fire events (See Table 2).

Five fire events were observed at four IMPROVE sites. Table 2 lists measured EC, OC, NO_3^-, K, soil and SO_4^{2-} concentrations (μg m^{-3}) and their ratios to averages. BC versus OC and K versus BC ratios were also calculated and listed in Table 2 to illustrate the application of our criteria. It was found that except

for monitor BRIS, all other sites (COHU, MACA and GRSM) had BC/OC and K/BC ratios comparable to the ratios of the same quantities due to biomass burning reported by other researchers (Reid et al., 2005; DeBell et al., 2004). BRIS is a coastal site likely influenced by sea salts (Fig. 4).

For the four identified fire cases, ΔCO as a modeled fire tracer around the IMPROVE site was plotted. Fire signals on June 21 at COHU and GRSM and on June 24 at MACA were reproduced in model simulation. The June 24 MACA case was used as an example (see Fig. 4).On June 24, 2013, detected fire spots were outside the SENEX domain, but SSW wind blew smoke plumes into the SENEX domain and affected modeled CO in MACA. Modeled ΔCO in MACA was 5 ppb.

Another IMPROVE site located upwind of MACA, CADI, was also potentially under the influence of that fire event; however, data from CADI on June 24 did not indicate a fire influence, possibly due to the frequency of IMPROVE sampling that eluded measurement or that the smoke plume was transported above the surface in disagreement with what was modeled. Within the four fire cases identified by the IMPROVE data during SENEX (Tab. 2), the model successfully captured three out of four events. The model missed fire signal on July 3 at MACA. The model missed the fire signal on July 3 at MACA. The following section is dedicated to the July 3 SENEX flight.

Plume Spatial Coverage

HMS determines fire hotspot locations associated with smoke and upon incorporating the smoke plume shape information from visible satellite images. HMS provides smoke plume shapefiles over much of North America, which is a two-dimensional smoke plume spatial depiction collapsing all plume stratifications to a satellite eye-view. For modeled plumes, we integrated modeled ΔCO by multiplying the layer values with the corresponding CMAQ model layer thicknesses and air density to derive a simulated smoke plume shape. HMS-derived smoke plume shape versus CMAQ predicted smoke plume shape was then used to evaluate the fire simulation.

Figure of Merits in Space (FMS) (Rolph et al., 2009) is a statistic for spatial analysis and was calculated as follows:

$$\mathrm{FMS} = \frac{\mathrm{Area\_hms} \cap \mathrm{Area\_cmaq}}{\mathrm{Area\_hms} \cup \mathrm{Area\_cmaq}} \mathrm{X}\ 100\%$$

Where Area_hms represents area of grid cells influenced by fire emission over CONUS detected by HMS and Area_cmaq represents area of grid cells over CONUS identified by model prediction. In general, a higher FMS value indicates a better agreement between the observed and modeled plume shape (Rolph et al., 2009).

Figure 5 summarizes FMS during the SENEX campaign. Average FMS was 22% with its maximum at 56% on July 6 and minimum at 1.2% on June 17 2013. Figure 6a exhibits HMS detected smoke plume and CMAQ calculated smoke plume over CONUS on July 6. The FMS score was 56% meaning that the modeled plume shape was consistent with that of HMS. However, HMS-BlueSky-Smoke emissions system might have underestimated the intensive fire influence areas along the border of California and Nevada. Subsequently, the model also under-predicted its associated influence in North Dakota, South Dakota, Minnesota, Iowa and Wisconsin.

Figure 6b exhibits the worst case on June 17 2013 in terms of resulting with a FMS score at 1.2%. Two reasons led to this: (i) CMAQ missed fire emissions from Canada. Those fire sources located outside the CONUS modeling domain and our simulation system used a climatologically-based static LBC; Secondly on June 17, there were a lot of fire hotspots in the Southeastern U.S., i.e., in Louisiana, Arkansas and Mississippi along the Mississippi River. Hotspots were detected but they lacked associated smoke in corresponding HMS imagery (Fig. 6c). This could be due to cloud blockage or to small agricultural debris clearing, burns in under-bushes or prescribed burns. These conditions prevented the HMS from identifying fires and hence emissions were not modeled for those sources.

It is noteworthy that the FMS evaluation contained uncertainties contributed from both modeled and observed values. The calculated campaign duration and SENEX-wide averaged FMS was 22%. It is significantly higher than that achieved by similar analyses done by HYSPLIT (Hybrid Single Particle Lagrangian Integrated Trajectory) smoke forecasting for the fire season of 2007 (6.1% to 11.6%) (Rolph et al., 2009). The primary reason is that the HYSPLIT smoke simulation is accessed at the invocation of a forecast cycle the HMS fire information which is already one day old due to retrieval latency and cycle-queuing issues. However, our model simulation in this study was from a retrospective module using current day HMS fire information. Such discrepancies have been discussed by Huang et al. 2019 (*manuscript in preparation*). The secondary reason is plume rise: despite both the HYSPLIT and CMAQ fire plume rise were estimated by the Briggs' equation, the HYSPLIT plume rise was limited to 75% of the mixed layer height (MLH) at daytime and two times MLH at nighttime, whereas the CMAQ fire plume rise did not have these limitations.

ASDTA

The Automated Smoke Detection and Tracking Algorithm (ASDTA) is a combination of two data sets: (1) the NOAA Geostationary satellite (G13) retrieves thermal enhancements aerosol optical depth due to fires using visible channels and produces a product called GOES Aerosol/Smoke Product (GASP) (Prados et al., 2007); and, (2) NOAA NESDIS HMS (Hazard Mapping System) fire smoke detection. First, the observation of the increase in AOD near the fire is attributed to the specific HMS fire; AOD values not associated with fires are dropped. Second, a pattern recognition scheme uses 30-minutes geostationary satellite AOD images to tracks the transport of this smoke plume away from the source. ASDTA provides the capability to determine whether the GASP is influenced by one or multiple smoke plumes over a location at a certain time.

ASDTA is originally generate to provide operational support for verification of the NOAA HYSPLIT dispersion model predicts smoke plume direction and extension (Draxler and Hess 1998). These data are also suitable for model performance evaluation in this study. For each simulation, modeled AOD was calculated for each sensitivity test ("with-fire" or "without-fire") and ΔAOD is defined as the difference obtained by subtracting AOD_without-fire from AOD_with-fire.

Figure 7a illustrates a GOES retrieved AOD (summed over from 10:00 am to 2:00 pm at local time) contour plot that reflects influences by smoke plumes over the CONUS domain on June 14 2013. Figure 7b presents similar results, but for simulated ΔAOD (with-fire – without-fire). For further evaluation of the HMS detected smoke plume shape Fig. 7c can be compared with Figs. 7a and 7b. Figure 7a shows several regions under the influence of fires in: California, northwest Mexico, Kansas, Missouri, Oklahoma, Arkansas, Texas and part of the Gulf of Mexico. In the northeastern USA, fire plumes occurred occasionally. Those regions agreed relatively well with the shaded contours between Figs. 7a and 7c. However, due to the lack of fire treatments in the CMAQ LBC, the simulation (Fig. 7b) missed smoke influence on the northeast region of the CONUS domain. CMAQ also failed to simulate the fire influences in the southwest region of the domain.

Similar plots for June 25 are shown in Figs. 7d, 7e and 7f for ASDTA, CMAQ and HMS, respectively. The ASDTA (Fig. 7d) diagnosed an overestimation in fire influences in the south including Texas and the Gulf of Mexico and an underestimation in the northeastern U.S. On the other hand, the model predicted two strong fire signals clearly: near the border between Arizona and Mexico, and in Colorado (See Fig. 7e). All the fire influenced areas in Fig. 7e were seen in observation by HMS in Fig. 7f.

Comparing ASDTA plots and CMAQ ΔAOD plots (Fig. 7a vs 7b; Fig. 7d vs 7e), both similarities and differences were found. Similarities were attributable to similar fire accounting and meteorology. Differences were attributable to: HMS contains more fire hotspots than those used by CMAQ due to

domain size; only fires inside the CONUS were included in the CMAQ fire simulation and LBCs did not vary to reproduce impacts of wildfires from outside of the domain.

SENEX

SENEX (Southeast Nexus) was a field campaign conducted by NOAA in cooperation with the US EPA and the National Science Foundation in June and July 2013. Although SENEX was not specifically designed for fire studies, its airborne measurements included $PM_{2.5}$ OC and EC, CO and acetonitrile (CH_3CN). CH_3CN was chosen as a fire tracer since it is predominantly emitted from biomass burning (Holzinger et al., 1999; Singh et al., 2012).

CH_3CN has a residence time in the atmosphere of around 6 months (Hamm and Warneck 1990) and the reported CH_3CN background concentration is around 100 - 200 ppt (Singh et al., 2003). Measured CH_3CN concentrations tend to increase with altitude (Singh et al., 2003; de Gouw et al., 2003), since biomass burning plumes tend to ascend during long-range transport. During SENEX, measured CH_3CN showed a similar pattern. Fire signals were identified through airborne measurements of CH_3CN when its concentration exceeded the background; e.g., on July 3 2013, or when its concentration peak appeared at high altitude; e.g., on June 16 2013 and July 10 2013.

CH_3CN airborne measurements were used to identify fire plumes at certain locations and heights during SENEX. For model evaluations, fire locations and accurate meteorological wind field are crucial to interpret 2-D measurements such as IMPROVE, HMS and ASDTA. To verify a 3-D fire field, it is critical to capture plume rise. However, it was extremely difficult to back out plume rise from the airborne measurements. An additional uncertainty arose in the difference of temporal resolutions of the data: IMPROVE, HMS shapefiles and ASDTA were daily or hourly data, whereas airborne CH_3CN data were measured at one-minute intervals.

Figure 8a shows a CMAQ simulated ΔCO vertical distribution along flight transects on June 16 2013. This flight occurred during the weekend over and around power plants around Atlanta, GA. The color of flight path represents observed CH_3CN concentration in ppt. In Fig. 8a, the concentration of ΔCO increased from surface to 5000 m, especially above 2000 m. Six CH_3CN concentration peaks were observed when AGL was above 2500 m.

For CMAQ simulated ΔCO, five out of six fire signals detected by CH_3CN measured spikes were captured where ΔCO concentrations were all above 3 ppb. Only one fire signal was missed by the model at 18:30 UTC June 16 2013. Model simulation showed that long range transports (LRT) of smoke plumes influenced airborne observations. Fire signals from the free troposphere subsided and influenced flight measurements. High EC or OC or CO did not concur with high CH_3CN observation probably due to species lifetime differences. HMS smoke plume did not show any hotspots or smoke plume around Atlanta suggesting that the sources of those observed fire signals were not from its vicinity.

A similar phenomenon was seen in SENEX flight 0710, which occurred during flight transects from Tennessee to Tampa, FL. Figure 8b is a similar graph as Fig. 8a. Based on ΔCO concentrations, CMAQ captured the July 10 case as fire signals were observed. Nonetheless, ΔCO may be over predicted at around 19 UTC. The model exhibited a fire signal with ΔCO concentration of about 3 ppb near 6000 m around 19 UTC, whereas measured CH_3CN was 120 ppt.

SENEX flight on July 3

Observations from IMPROVE, HMS and SENEX identified fire signals on July 3 2013. ASDTA retrievals were not available. Those signals were missed by the model. In this section, all of evaluation methods addressed above were used to study potential causes of failure of the model to reproduce fire signals.

At the MACA IMPROVE site on July 3 2013, the wind direction at the surface was southeasterly, with no fire hotspots (solid black circle) located upwind of MACA (Fig. 9a). Without any identified hotspots upwind, the model missed fire signals observed at MACA on July 3 2013.

Flight #0703 was a night mission targeting power plants in Missouri and Arkansas. The flight path is shown in Fig. 9b and is colored by measured CH_3CN concentration. In order to highlight CH_3CH concentrations above 400 ppt in the measurements, CH_3CN concentrations below 400 ppt were represented by black dots. During the flight, 16 measurements of acetonitrile concentration above 400 ppt were observed and the maximum was 3227.9 ppt. These observations were located over northwestern Tennessee and close to the borders of Kentucky, Illinois, Missouri and Arkansas. Except for one observation, the flight ASL was between 500 m and 1000 m.

Enhancements of CO and OC were also measured concurrently with CH_3CN. Figures 9c and 9d show scatter plots for CH_3CN versus CO and OC, respectively. Measured CH_3CN was highly correlated to both measured CO and OC, with linear correlation coefficients (R^2) of 0.83 and 0.71, respectively. The $\Delta CH_3CN/\Delta CO$ ratio is around 2.7 (ppt/ppb), which is consistent with findings of other measurements over California in 2002 when a strong forest fire signal was intercepted by aircraft (de Gouw et al., 2003). The $\Delta CH_3CN/\Delta OC$ ratio was around 6.85 (ppt/(mg m^{-3})), which is also in the range of biomass burning analyses in MILAGRO (Megacity Initiative Local and Global Research Observations) (Aiken et al., 2010).

Figure 9e shows model simulated ΔCO with peaks at AGL below 3000 m. Fire signals showed substantial influences on aircraft measurement at around 5 UTC. However, clear fire signals between 2 UTC and 3 UTC were observed based on prior CH_3CN analysis. The model either predicted insufficient fire emission influences or missed it. FMS score on July 3 was 30%. Figure 9f shows that CMAQ did not predict plumes where the HMS plume analysis exhibited several dense smoke plumes. As NOAA Smoke

Text Product (http://www.ssd.noaa.gov/PS/FIRE/DATA/SMOKE) described on its July 03 0501 UTC report: a smaller very dense patch of remnant smoke, analyzed earlier the same day over southern Missouri, drifted southward into Arkansas."

The reasons the model missed these fire observations were not clear. Figures 10, 11a and 11b suggest a few clues. Figure 10 is a backward trajectory analysis plot for the observations obtained during the SENEX flight on July 3 with CH_3CN measured concentration above 400 ppt. Both transect and passing altitude of the air parcels clearly showed those measurements were most likely influenced by the nearby pollution sources. Figure 11a illustrates the locations of fire used in the CMAQ simulation. It is noted that hmshysplit.txt is input into BlueSky after HMS quality control (Fig. 1). There were several hotspots around the region where the IMPROVE site MACA was located and where the SENEX flight overpassed. Our fire simulation system might have underestimated smoke emissions from those fires. Other explanation was from Fig. 11b, which illustrated hotspots in hmx.txt. In hmx.txt, every detected fire spots by HMS before quality control were showed. Comparing Fig. 11a with 11b, there were clusters of fire spots in the central U. S. especially in West Tennessee. However, those spots were removed during the HMS quality control process because there were no associated smoke plumes visible. In most of times, those fires were believed to be small sized fires such as from agriculture fires or prescribed burns. For this case, there seem to have been thin clouds overhead and thicker clouds in the vicinity, (http://inventory.ssec.wisc.edu/inventory/image.php?sat=GOES-13&date=2013-07 03&time=16:02&type=Imager&band=1&thefilename=goes13.2013.184.160147.INDX&coverage=CONUS &count=1&offsettz=0), so it would be hard to differentiate smoke from clouds by satellite observations

CONCLUSIONS

In support of the NOAA SENEX field experiment in June-July 2013, simulations were conducted including smoke emissions from fires. In this study, a system accounting for fire emissions in a chemical transport model is described, including a satellite fire detecting system (HMS), a fire emission calculation model (BlueSky), a pre-processing of fire emissions (SMOKE), and simulation over the SENEX domain by CMAQ. The focus of this work is to evaluate the system's capability to capture fire signals identified by multiple observation data sets. These data sets included IMPROVE ground station observations, satellite observations (HMS plume shapefile and ASDTA) and airborne measurements from the SENEX campaign.

For IMPROVE data, potential fire signals were identified by measured potassium concentrations in $PM_{2.5}$. Fire identifications in CMAQ rely on predicted ΔCO, the difference between simulations with and without fire emissions. Three out of four observed fire signals were captured by CMAQ simulations. For HMS smoke plume shapefiles that were manually plotted by analysts to represent the regions impacted by smoke, we used FMS to calculate the percentage of its overlapping with CMAQ predicted smoke plumes. FMS averaged 22% over forty days of the SENEX campaign. In terms of fire smoke impacts on ΔAOD, both ASDTA and CMAQ showed patterns that were compared to HMS plume shapefile. In terms of measured CH_3CN, a biomass burning plume tracer, both SENEX aircraft in-flight measurements and CMAQ simulations captured signatures of long range transport of fire emissions from elsewhere in the CONUS domain.

Generally, using HMS-detected fire hotspots and smoke data was useful for predictions of fire impacts and their evaluation. The HMS-BlueSky-SMOKE-CMAQ fire simulation system, which is also used in NAQFC, was able to capture most of the fire signals detected by multiple observations. However, the system failed to identify fire cases on June 17 and July 3 2013 -- thereby demonstrating two problems with the simulation system. One identified problem was the lack of a dynamical fire LBC bounding the

CONUS domain to represent the inflows of strong fire signals originating from outside the simulation domain. Secondly, the HMS quality control procedure eliminated fire hotspots that were not associated with visible smoke plumes leading to an underestimation.

We were keen on understanding and quantifying the various uncertainties and observational constraints of this study therefore the following rules of thumb were observed: (1) a holistic evaluation approach was adopted so that the fire smoke algorithm was interpreted as a single entity to avoid deadlock due to over-interpretation of uncertainty of the single component in the system; (2) analysis conclusion applicable to the entire simulation period was drawn so that the episodic characteristics of the cases embedded in the simulation were averaged and generalized. This new methodology may benefit NAQFC; (3) we took advantage of the multiple perspectives of the observation systems that offered a wide spectrum of temporal and spatial variabilities intrinsic to the systems; (4) we were intentionally conservative in discarding data so that we maximized the sampling pool for statistical analysis and avoided unwittingly discarding poorly simulated cases, good outliers, and weak but accurate signals.

Quantitative evaluation of fire emissions and their subsequent influences on ozone and particulate matter in this fire and smoke prediction system is challenging. Future work includes applying these findings to the NAQFC and improving the NAQFC system's capabilities to simulate fires accurately.

Code Availability

The source code used in this study is available online at http://www.nco.ncep.noaa.gov/pmb/codes/nwprod/cmaq.v5.0.2.

Acknowledgements & disclaimer

This work was partially funded by the NASA Air Quality Applied Sciences Team (AQAST), project grant NNH14AX881. The authors are thankful to Dr. Joost De Gouw and Dr. Martin G. Graus of the Earth System Research Laboratory, NOAA for sharing the SENEX campaign data used in this study. Although this work has been reviewed by the Air Resources Laboratory, NOAA and approved for publication it does not necessarily reflect their policies or views.

Figures:

Figure 1, schematics of fire emission and smoke plume simulation system used: Data-feed and/or modeling of physical and chemical processes were handled largely sequentially from top to bottom and from left to right; The right hand four vertical boxes depict the submodel names: NESDIS Hazard Mapping System (HMS) for wild fire hot spot detection; US Forest Service's BlueSky for fuel type and loading parameterization; and US EPA's Sparse Matrix Operator Kernel (SMOKE) to handle emission characterization; and lastly the Community Multiple-scale Air Quality model (CMAQ) was applied to simulate the transformation, transport and depositions of the atmospheric constituents. The "SENEX" in-set framed by red emboldened lines was the domain for this study.

Figure 2, in 4km SENEX domain, (a): the contribution (%) of CO emission from fires occurred inside the SENEX domain; (b): the contribution (%) of CO flux flowing into the SENEX domain from its boundary caused by fires burning outside the SENEX domain but inside the CONUS domain.

Figure 3, CMAQ simulated ΔCO (ppb): i.e., the CO concentration difference between CMAQ simulation with and without fire emissions, extracted along the overall SENEX flight paths during the SENEX campaign between June 10 and July 20 2013.

Figure 4, simulated ΔCO (>2.0 ppb) in the SENEX domain on June 24 2013 at 20:00 UTC overlaid with 2 m wind arrows with a 10 m s^{-1} reference arrow shown in the bottom right. The solid black circle is detected fire hotspots by HMS. The solid triangles labeled with station code represents IMPROVE sites used in model verification calculations.

Figure 5, FMS (Figure of Merits in Space) (%) from June 11 to July 19 in 2013 during the SENEX campaign.

Figure 6, Daily HMS observed plume shape versus CMAQ predicted daily averaged plume shape on (a): July 6 2013; (b): June 17 2013; The light blue shading represents modeled plume shape (defined as total column ΔCO) and the thin dash line and emboldened green lines encircle areas representing HMS-derived light and strong influenced plume shape, respectively. (c): HMS observed fire hotspots (red) and plume shapes (white) (http://ready.arl.noaa.gov/data/archives/fires/national/arcweb) on June 17, 2013.

Figures 7, GOES detected AOD influenced by fires using ASDTA diagnose method (summed over from 10:00 am to 2:00 pm local time). Color-shaded region represents the fire-smoke influenced areas and the color denotes the magnitude of the retrieved AOD on (a): June 14 2013; (d): June 25 2013; simulated ΔAOD (withfire – nofire) calculated by CMAQ on (b): June 14 2013; (e): June 25 2013; HMS observed fire hotspots (red) and plume shapes (white) on (c): June 14 2013; (f): June 25 2013.

Figure 8, vertical distributions of CMAQ simulated ΔCO (ppb) shown along flight transect on (a): June 16 2013; (b): July 10 2013; the x-axis label is UTC (hour) and y-axis label is AGL (m). Two color bars represent observed CH3CN concentration (filled square dots and rectangle bar in ppt) and simulated ΔCO concentration (backdrop color shading and fan bar in ppb), respectively.

Figure 9, plots for July 3 2013 case, (a): IMPROVE; (b): the flight path of SENEX #0703 colored by measured CH_3CN concentration (ppt); (c): CH_3CN (ppt) vs CO (ppb); (d): CH_3CN (ppt) vs AMS_Org (mg m^{-}

^{3}); (e): CMAQ simulated ΔCO vertical distributions along flight transect; (f): HMS observed plume shape versus CMAQ prediction.

Figure 10, a backward trajectory analysis for CH_3CN concentration in ppt greater than 400 ppt measured along a SENEX flight on July 03 in: (upper) aerial, and (lower) time vertical cross-sections.

Figure 11, detected fire hotspots on July 03 2013 as daily composite (a): hmxhysplit.txt; (b): hmx.txt.

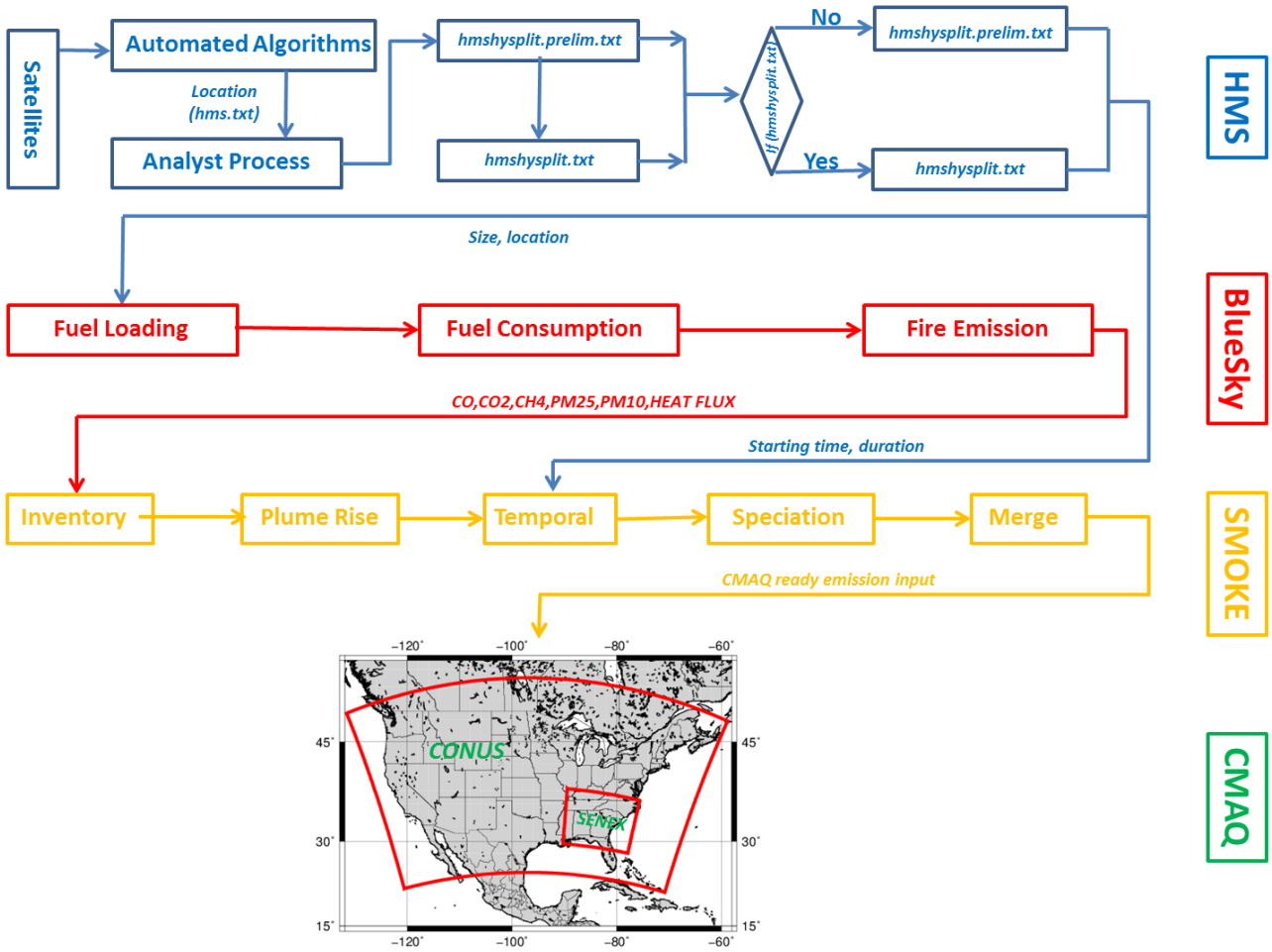

Figure 1: schematics of fire emission and smoke plume simulation system used: Data-feed and/or modeling of physical and chemical processes were handled largely sequentially from top to bottom and from left to right; The right hand four vertical boxes depict the submodel names: NESDIS Hazard Mapping System (HMS) for wild fire hot spot detection; US Forest Service's BlueSky for fuel type and loading parameterization; and US EPA's Sparse Matrix Operator Kernel (SMOKE) to handle emission characterization; and lastly the Community Multiple-scale Air Quality model (CMAQ) was applied to simulate the transformation, transport and depositions of the atmospheric constituents. The "SENEX" in-set framed by red emboldened lines was the domain for this study.

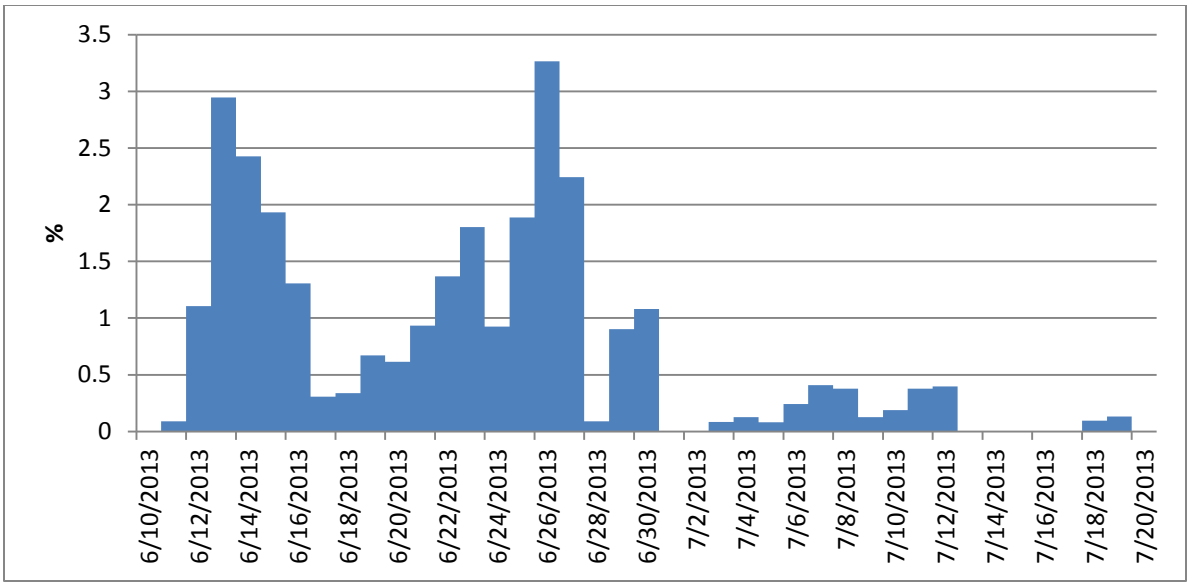

Figure 2a: the contribution (%) of CO emission from fires occurred inside the SENEX domain.

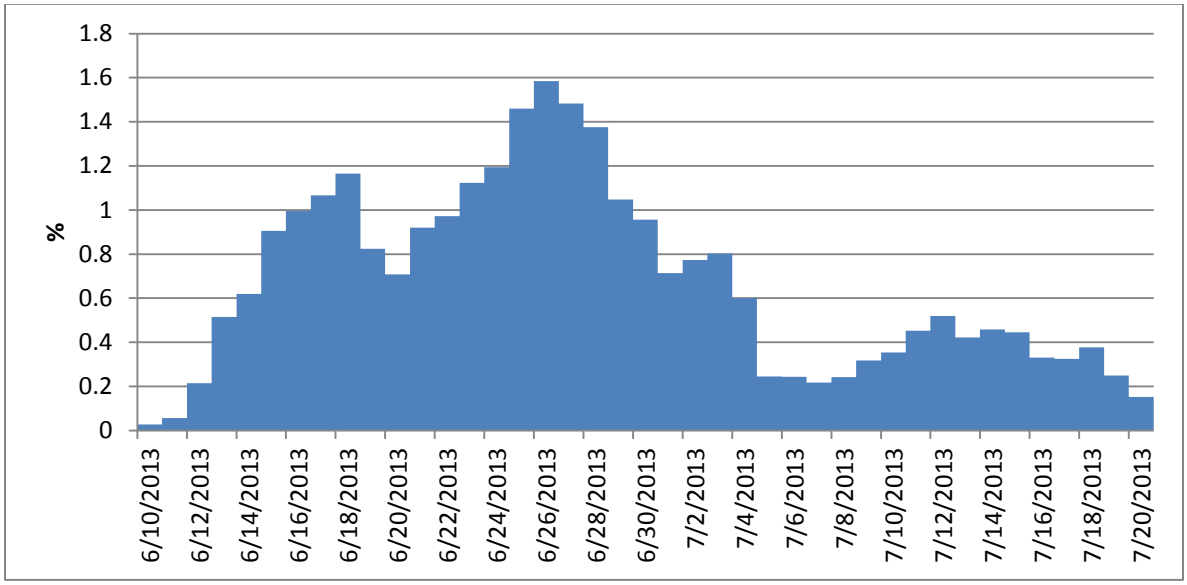

Figure 2b: the contribution (%) of CO flux flowing into the SENEX domain from its boundary caused by fires burning outside the SENEX domain but inside the CONUS domain.

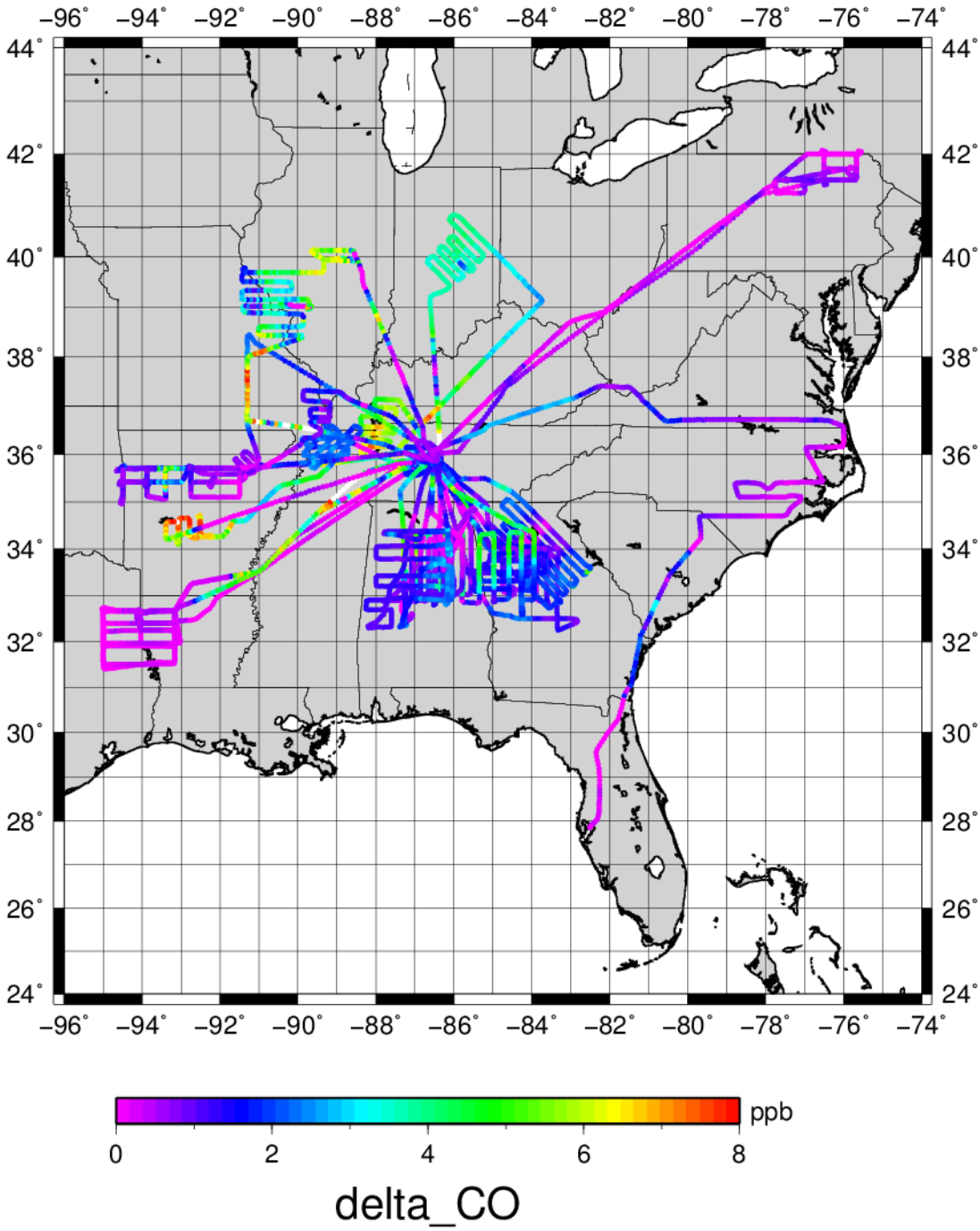

Figure 3: CMAQ simulated ΔCO (ppb): i.e., the CO concentration difference between CMAQ simulation with and without fire emissions, extracted along the overall SENEX flight paths during the SENEX campaign between June 10 and July 20 2013.

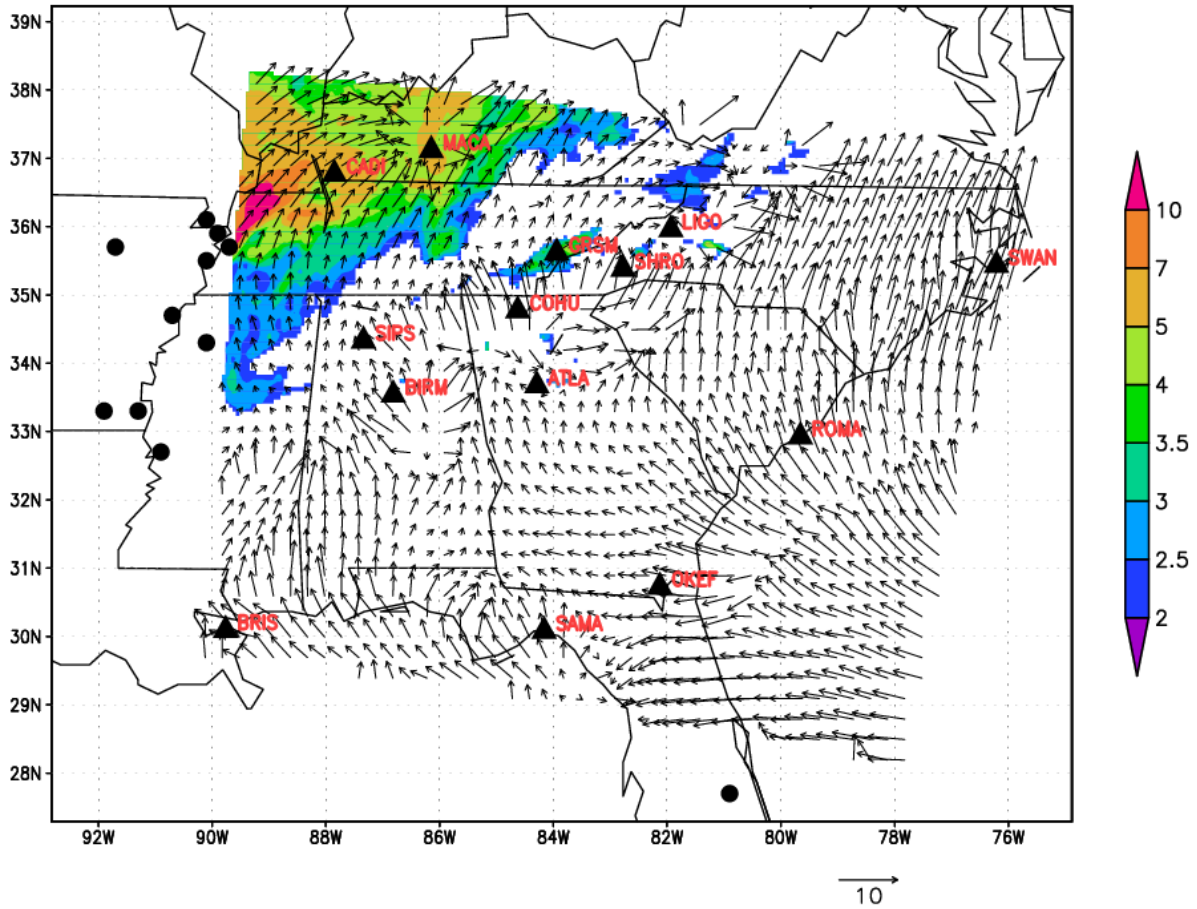

Figure 4: simulated ΔCO (>2.0 ppb) in the SENEX domain on June 24 2013 at 20:00 UTC overlaid with 2 m wind arrows with a 10 m s^{-1} reference arrow shown in the bottom right. The solid black circle is detected fire hotspots by HMS. The solid triangles labeled with station code represents IMPROVE sites used in model verification calculations.

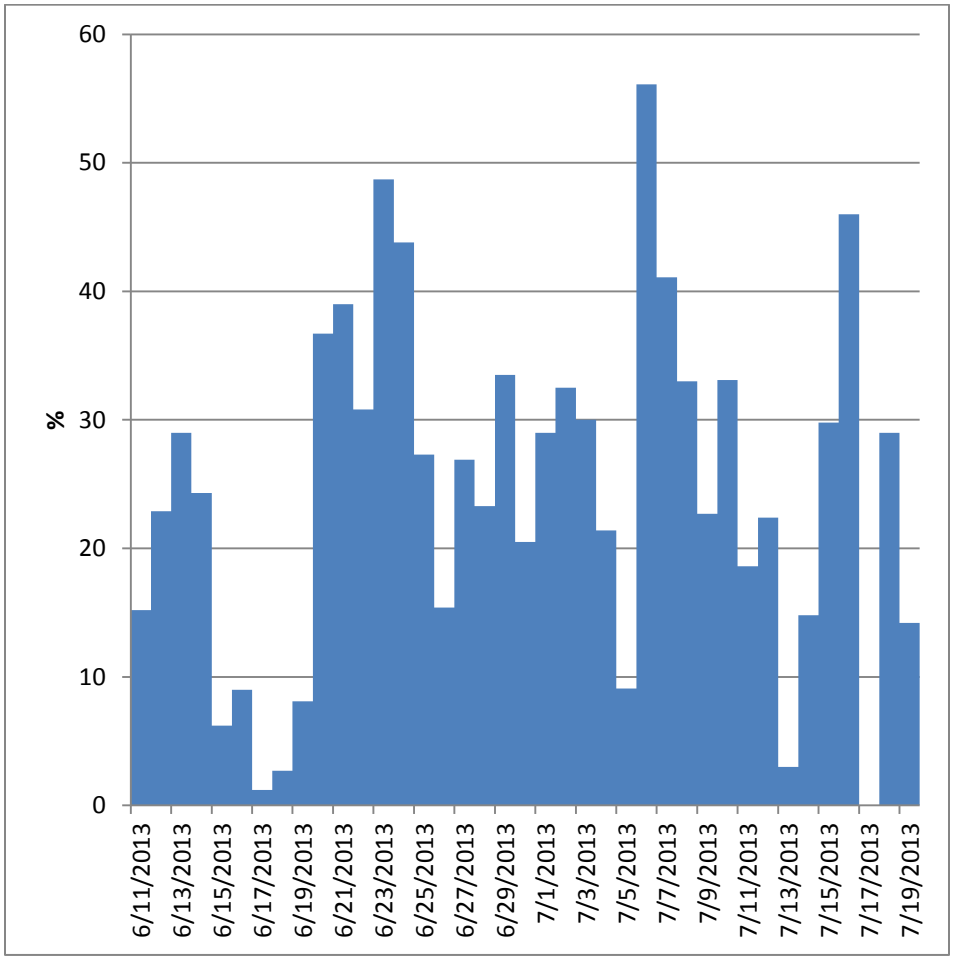

Figure 5: FMS (Figure of Merits in Space) (%) from June 11 to July 19 in 2013 during the SENEX campaign.

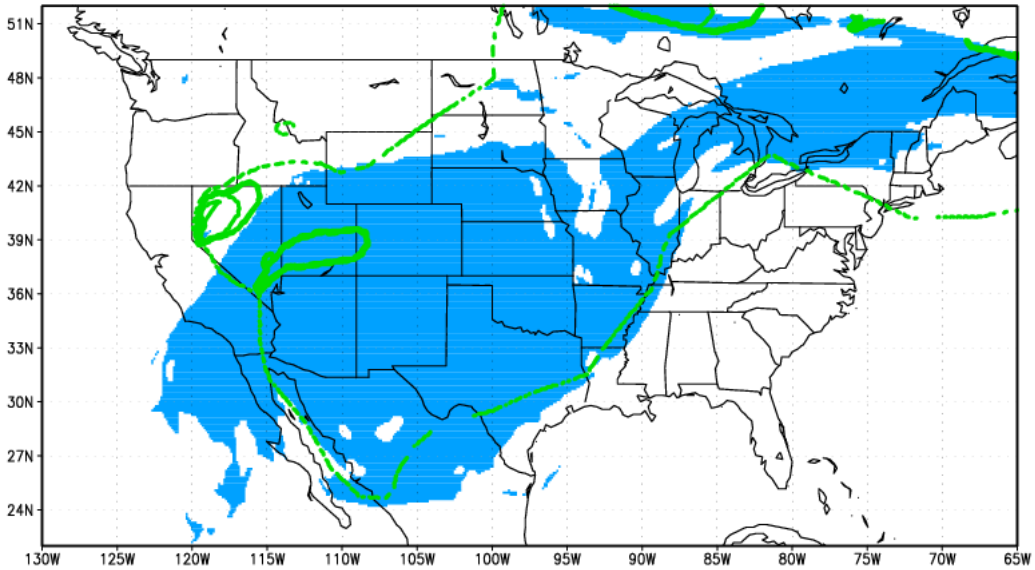

Figure 6a: Daily HMS observed plume shape versus CMAQ predicted daily averaged plume shape on July 6 2013; The light blue shading represents modeled plume shape (defined as total column ΔCO) and the thin dash line and emboldened green lines encircle areas representing HMS-derived light and strong influenced plume shape, respectively.

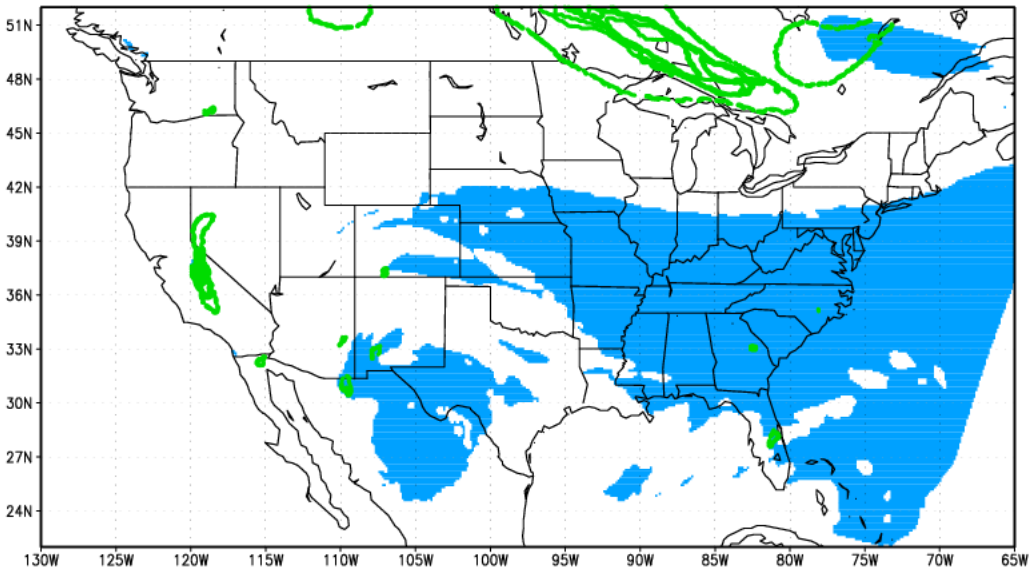

Figure 6b: same as Figure 6a but for June 17 2013.

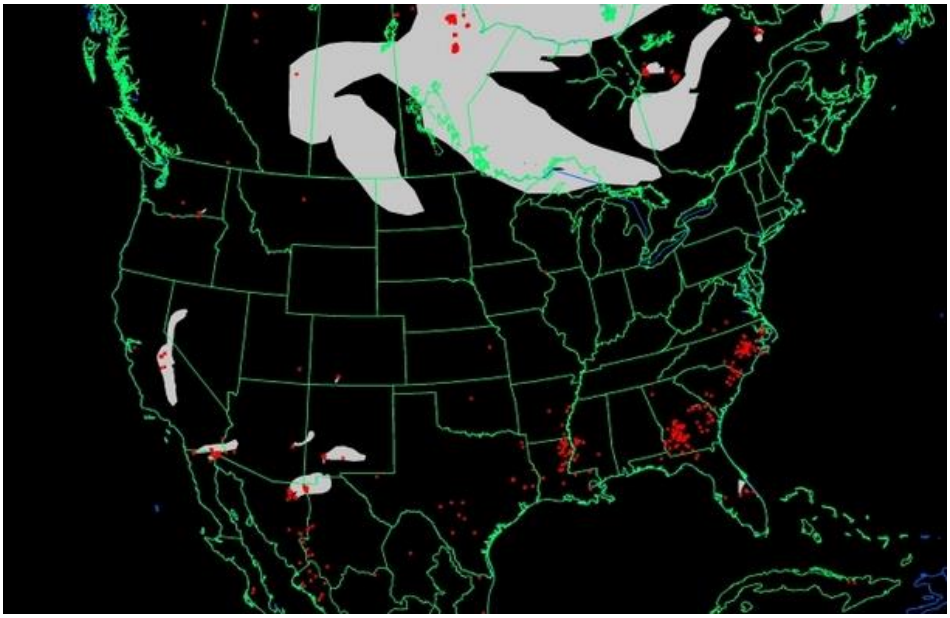

Figure 6c: HMS detected fire hotspots (red) and smoke plume shapes (white) on June 17 2013 (analysis day: 20130717, map generated: around 1100 GMT). (http://ready.arl.noaa.gov/data/archives/fires/national/arcweb).

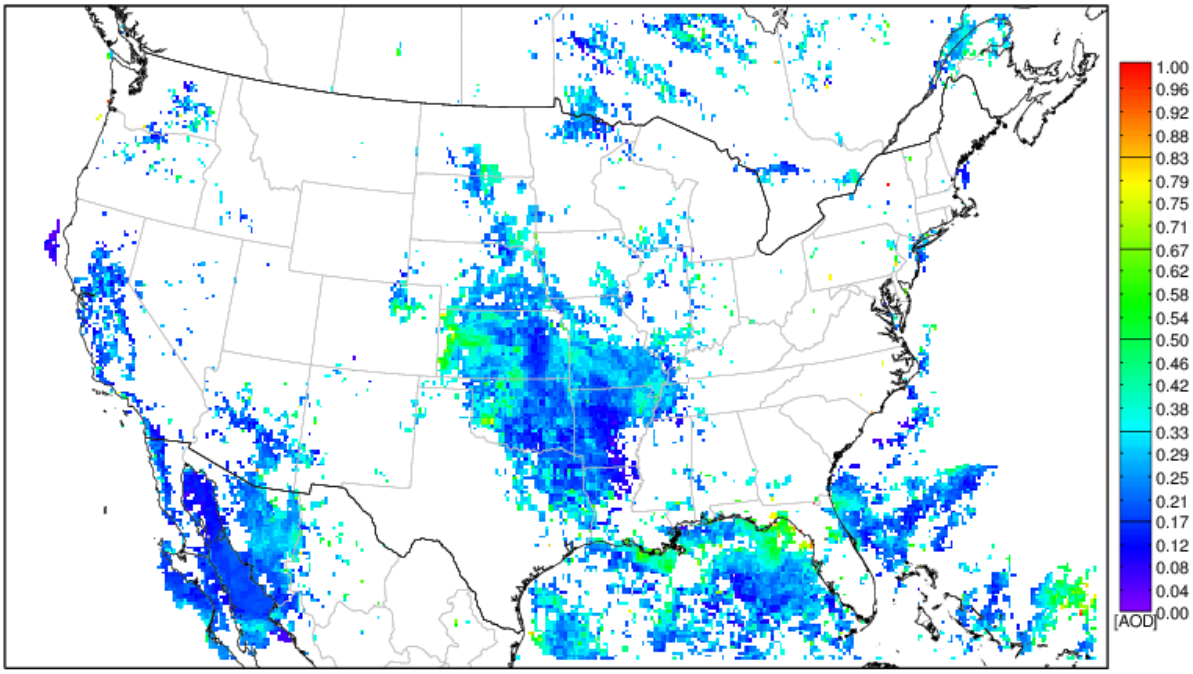

Figure 7a: GOES detected AOD influenced by fires using ASDTA diagnose method on June 14 2013 (summed over from 10:00 am to 2:00 pm local time). Color-shaded region represents the fire-smoke influenced areas and the color denotes the magnitude of the retrieved AOD.

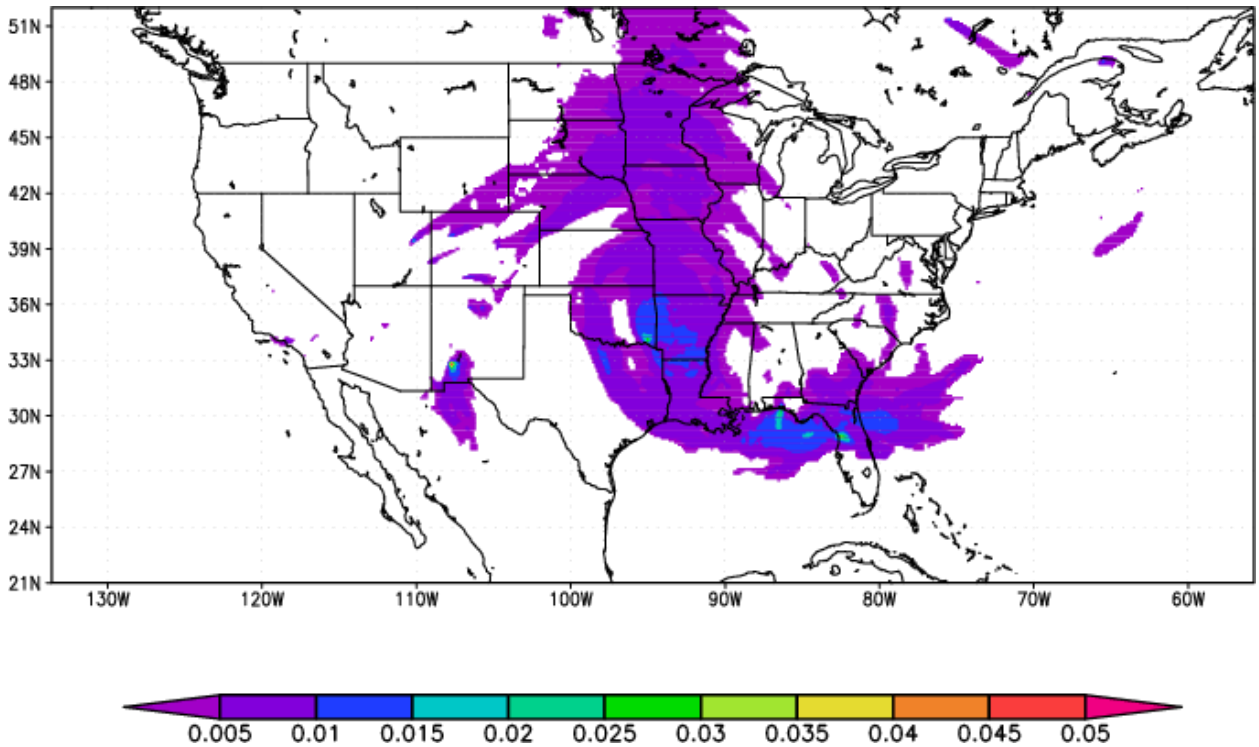

Figure 7b: simulated ΔAOD (with-fire – without-fire) calculated in CMAQ on June 14 2013.

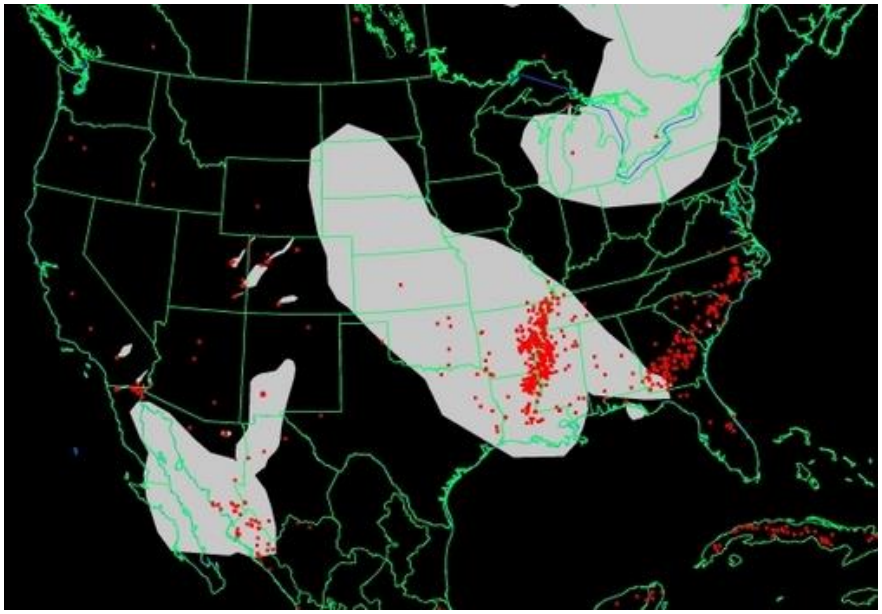

Figure 7c: same as Figure 6c but for June 14 2013.

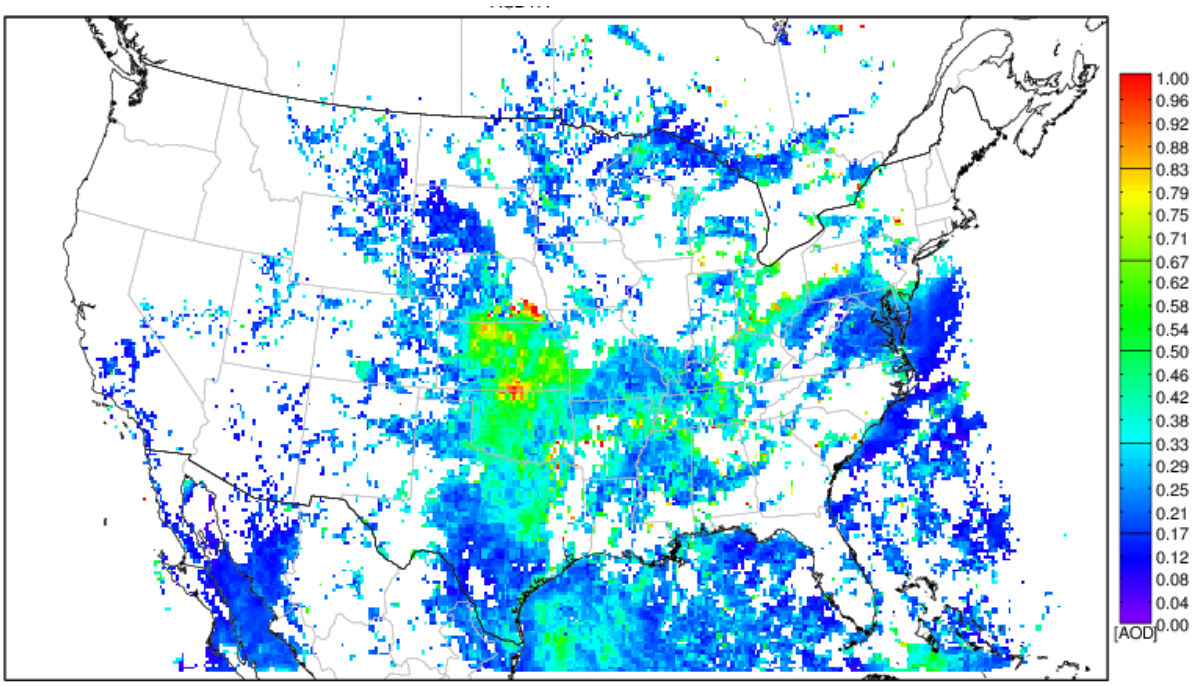

Figure 7d: same as Figure 7a but for June 25 2013.

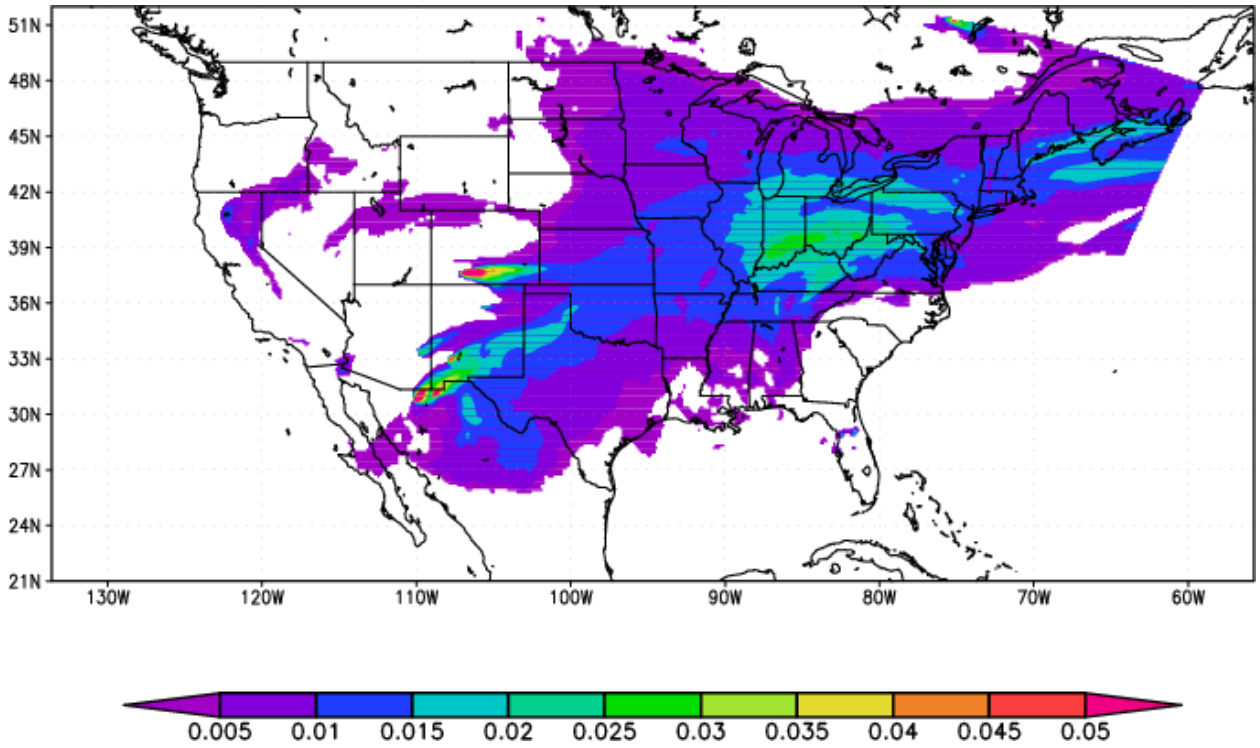

Figure 7e: same as Figure 7b but for June 25 2013.

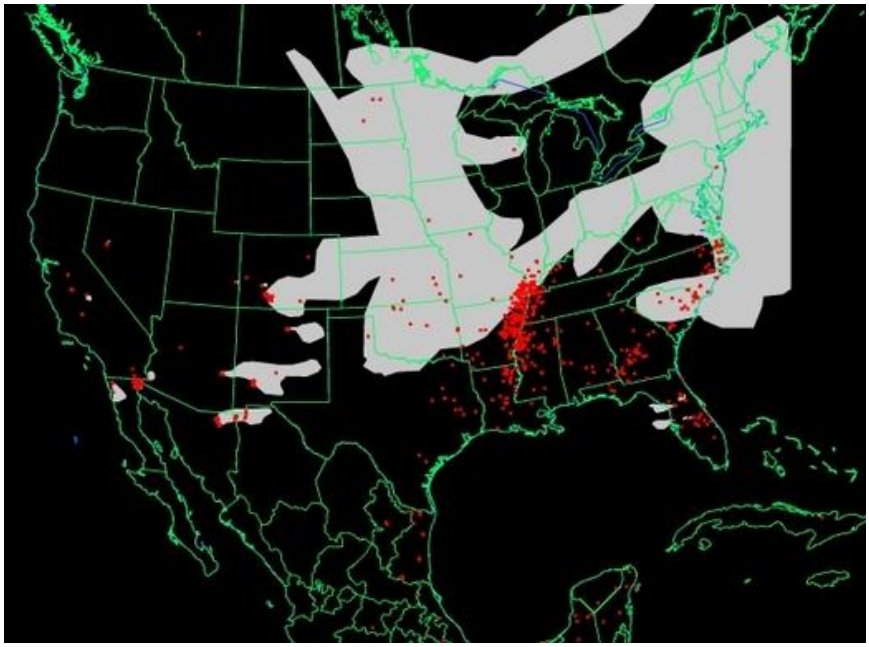

Figure 7f: same as Figure 6c but for June 25 2013.

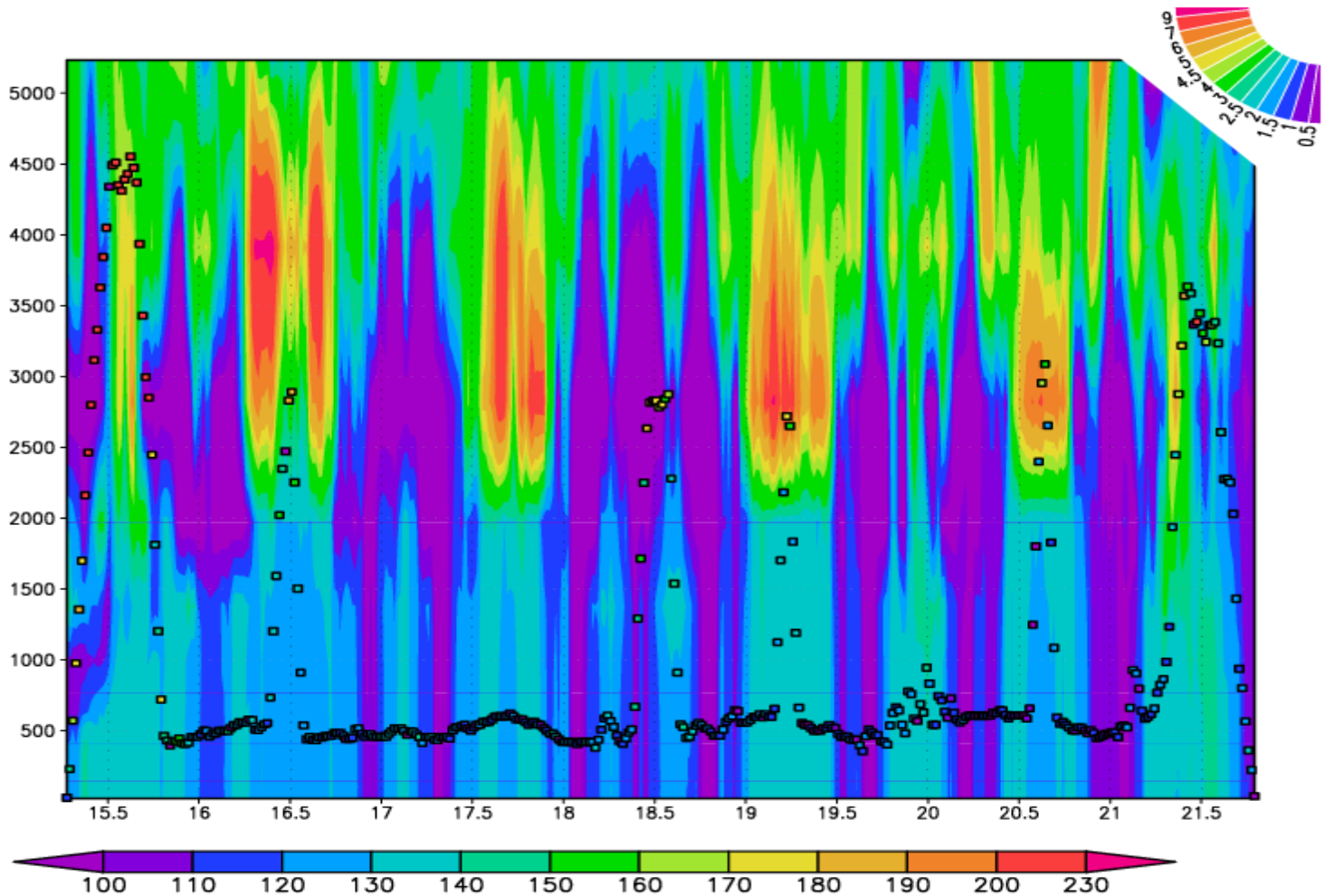

Figure 8a: vertical distributions of CMAQ simulated ΔCO (ppb) shown along flight transect on June 16 2013. The x-axis label is UTC (hour) and y-axis label is AGL (m). Two color bars represent observed CH_3CN concentration (filled square dots and rectangle bar in ppt) and simulated ΔCO concentration (backdrop color shading and fan bar in ppb), respectively.

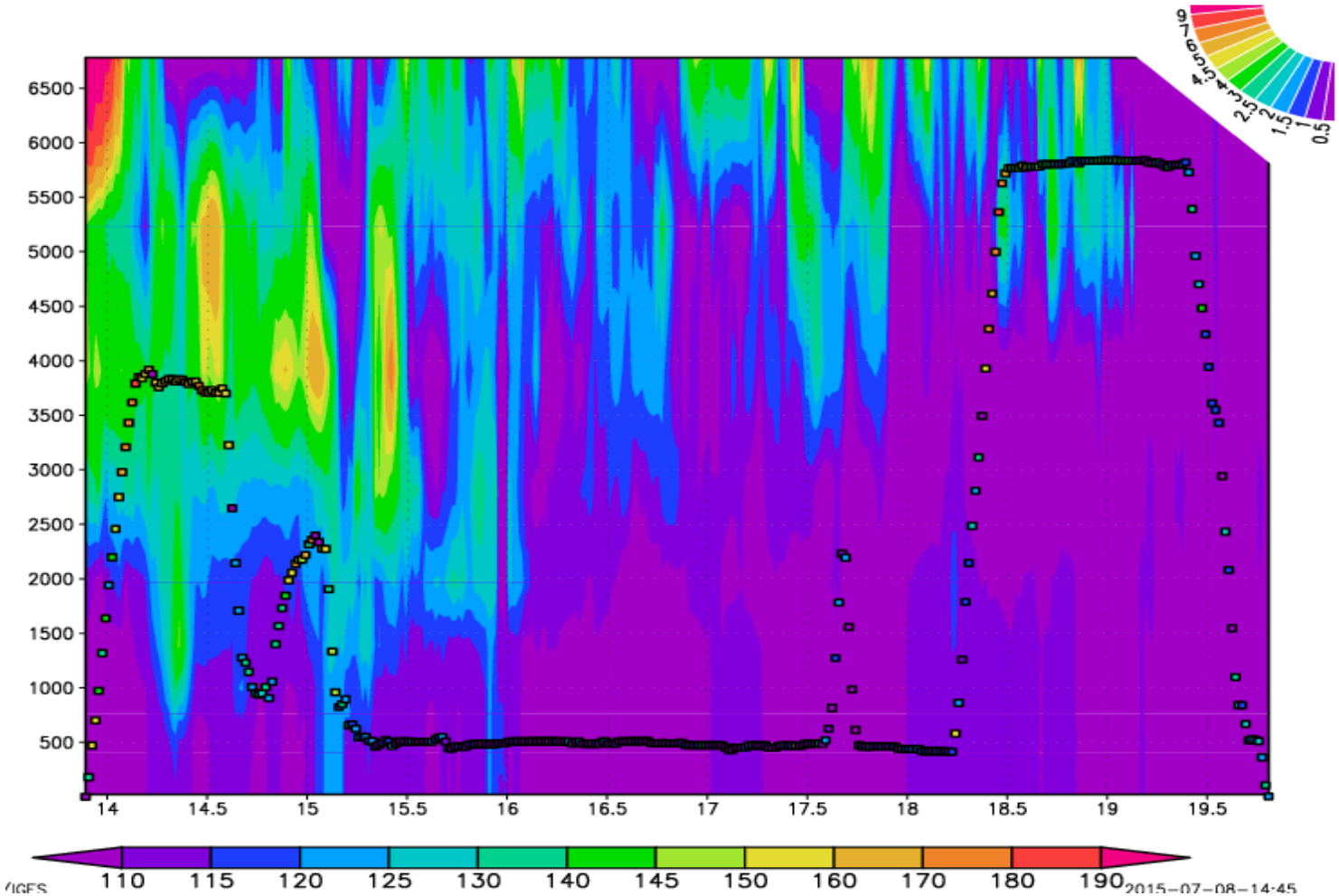

Figure 8b: same as Figure 8a but for July 10 2013.

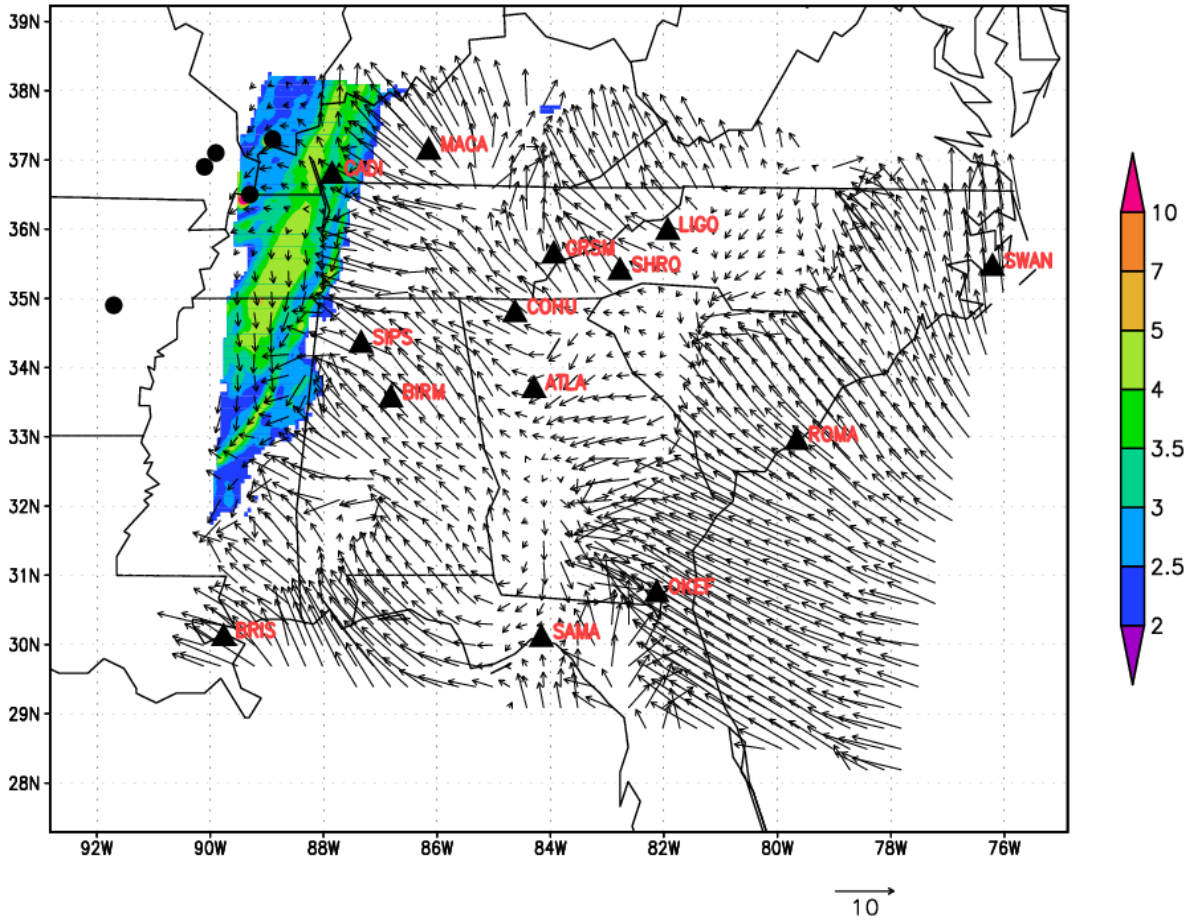

Figure 9a: same as Figure 4 but for July 03 2013.

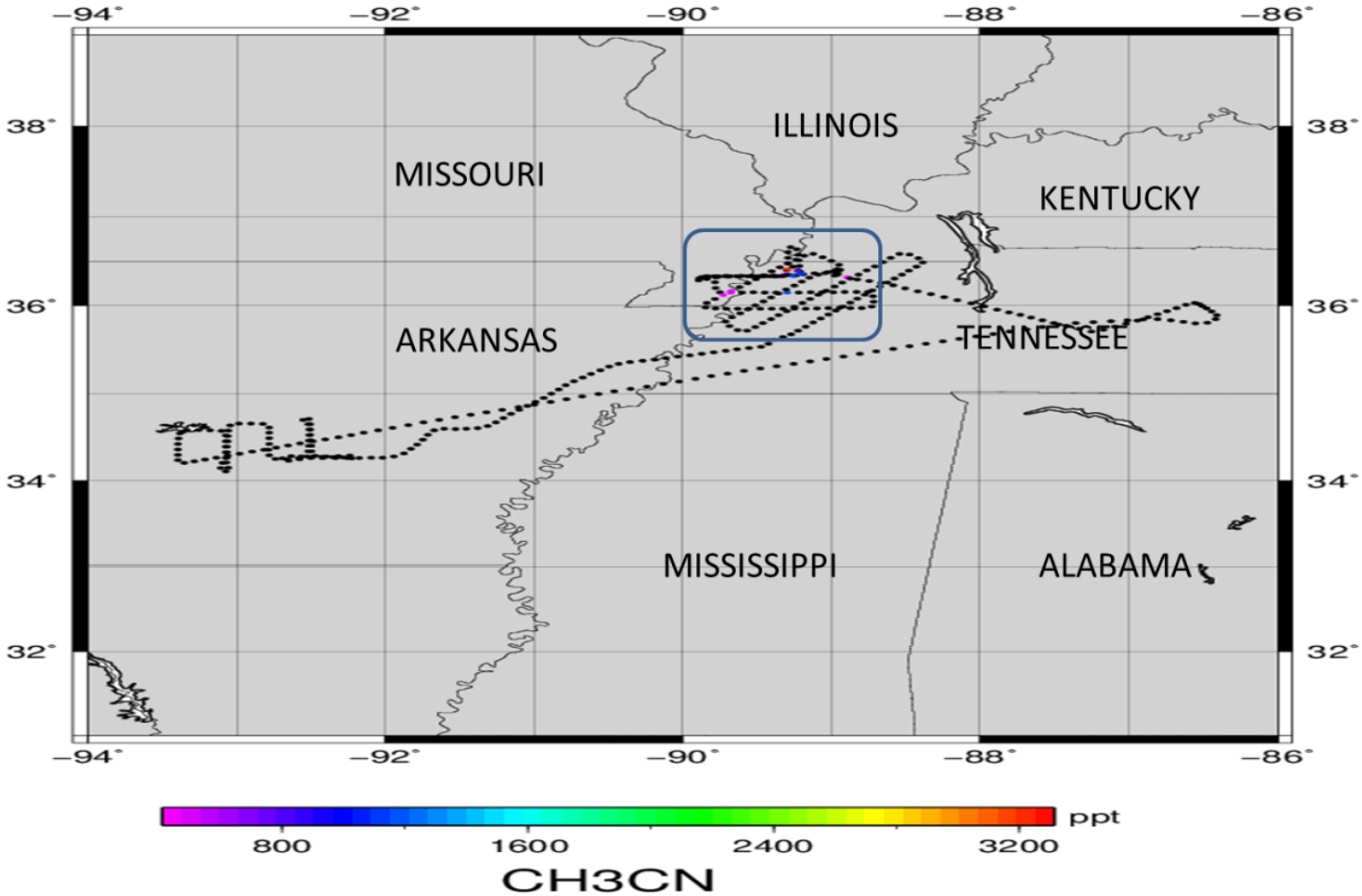

Figure 9b: the flight path of SENEX #0703 traversed the Central Plain between local time 10:00pm and 11:00pm on July 02, 2013 --- colored by measured CH3CN concentration (ppt).

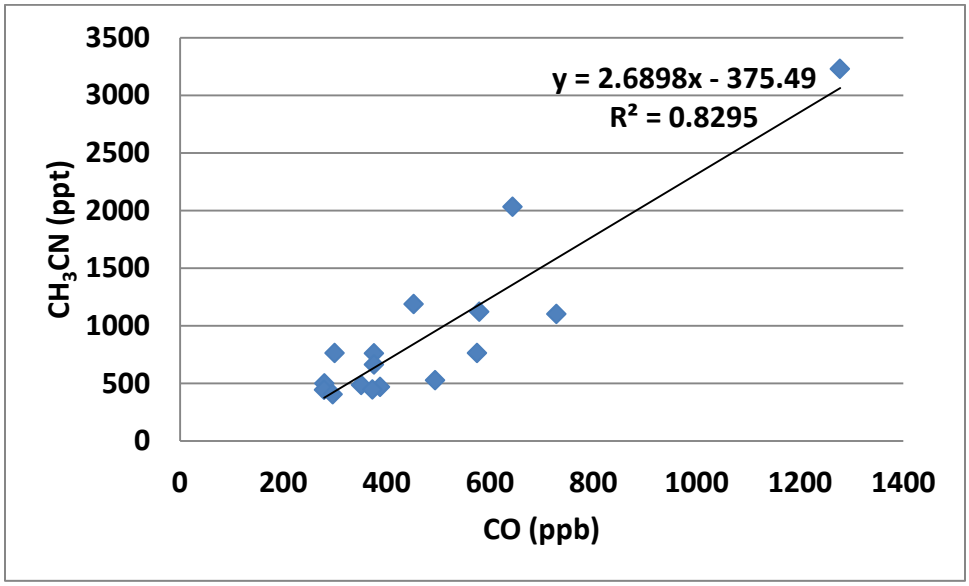

Figure 9c: CH_3CN (ppt) vs CO (ppb) scatter plot.

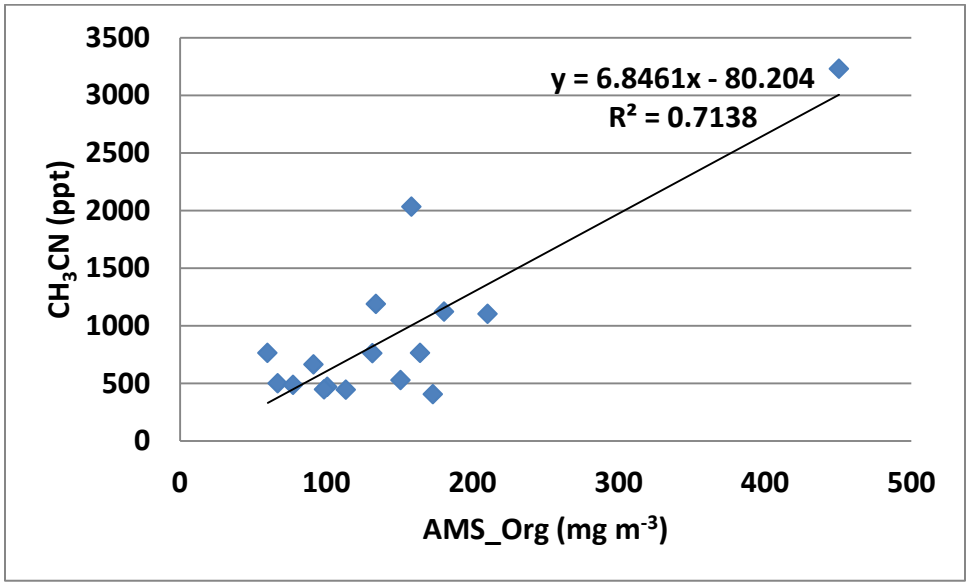

Figure 9d: CH_3CN (ppt) vs AMS_Org (mg m^{-3}) scatter plot.

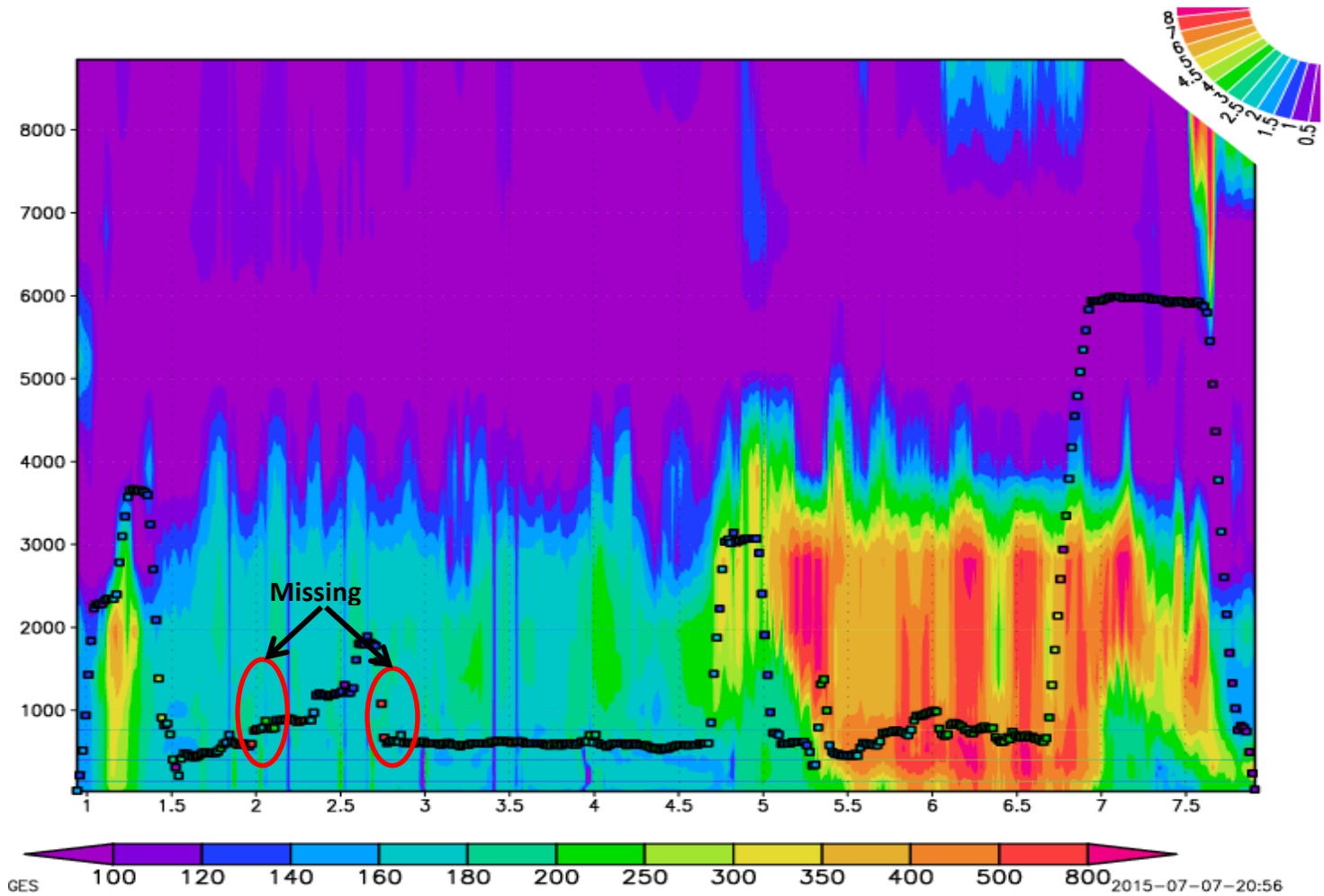

Figure 9e: same as Figure 8a but for July 03 2013. The emboldened red ovals highlighted missing CH_3CN concentration measurements.

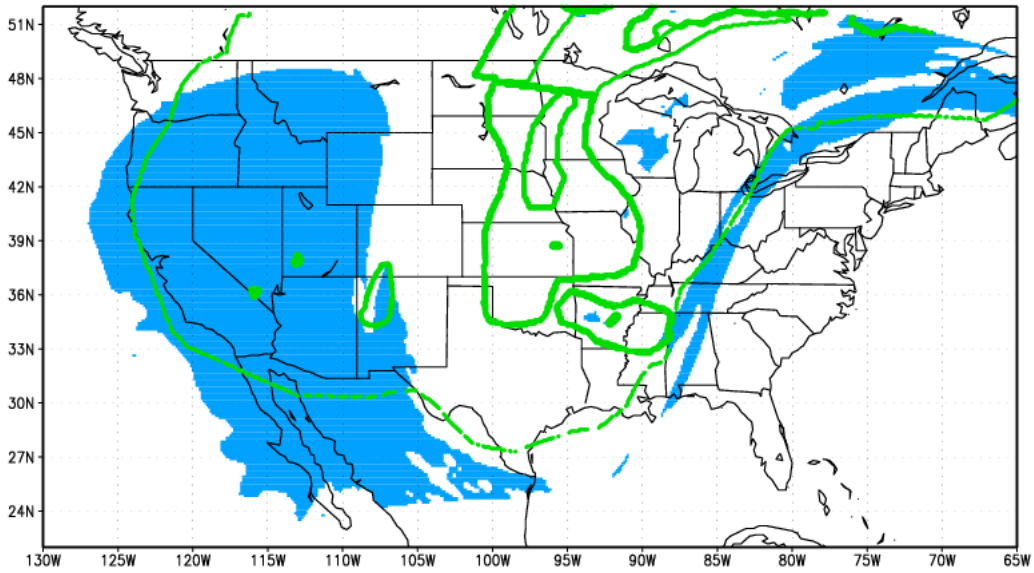

Figure 9f: same as Figure 6a but for July 03 2013.

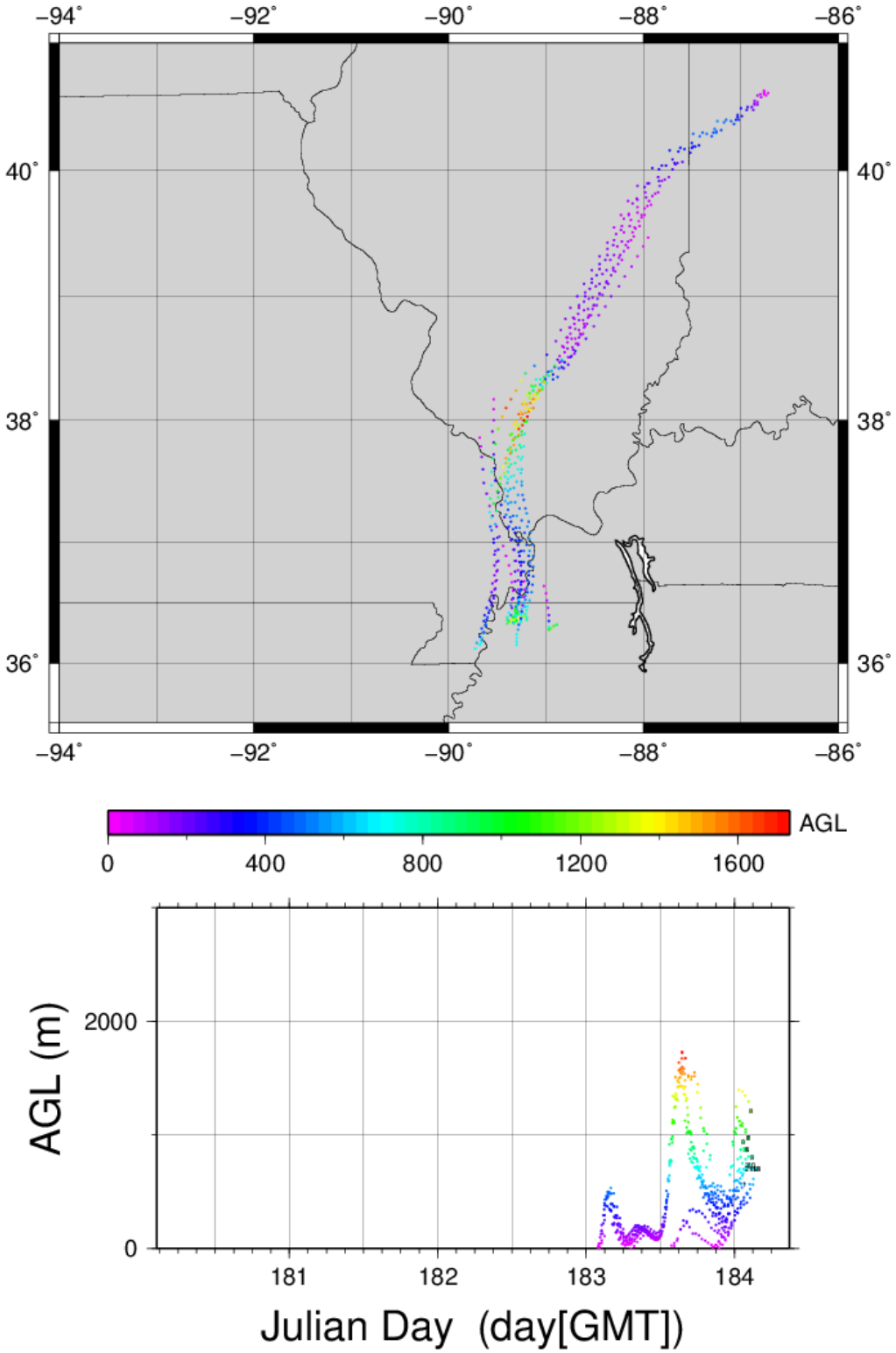

Figure 10: a backward trajectory analysis for CH_3CN concentration in ppt greater than 400 ppt measured along a SENEX flight on July 03 in: (upper) aerial, and (lower) time vertical cross-sections.

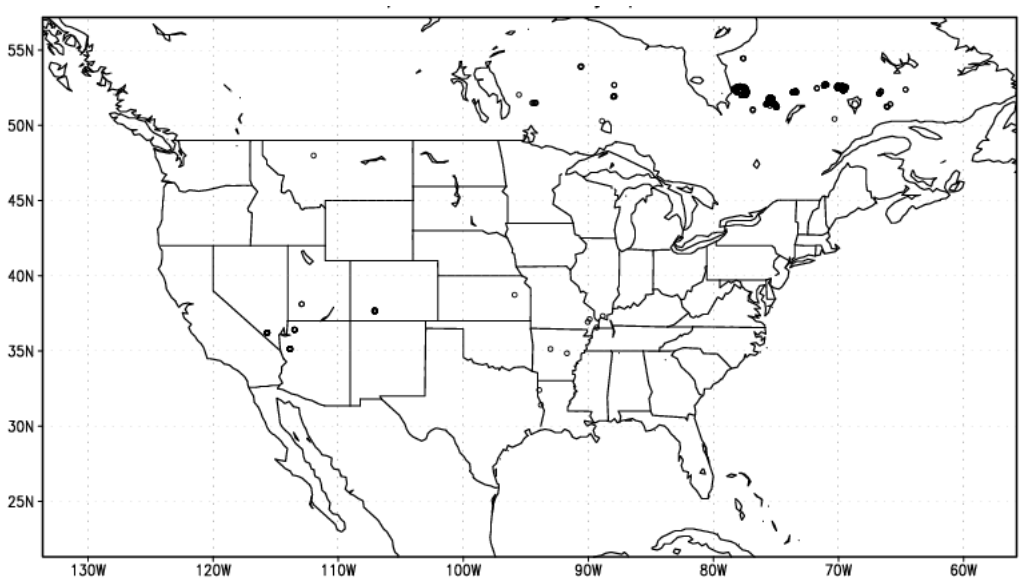

Figure 11a: fire hotspots in hmxhysplit.txt on July 03 2013 as daily composite.

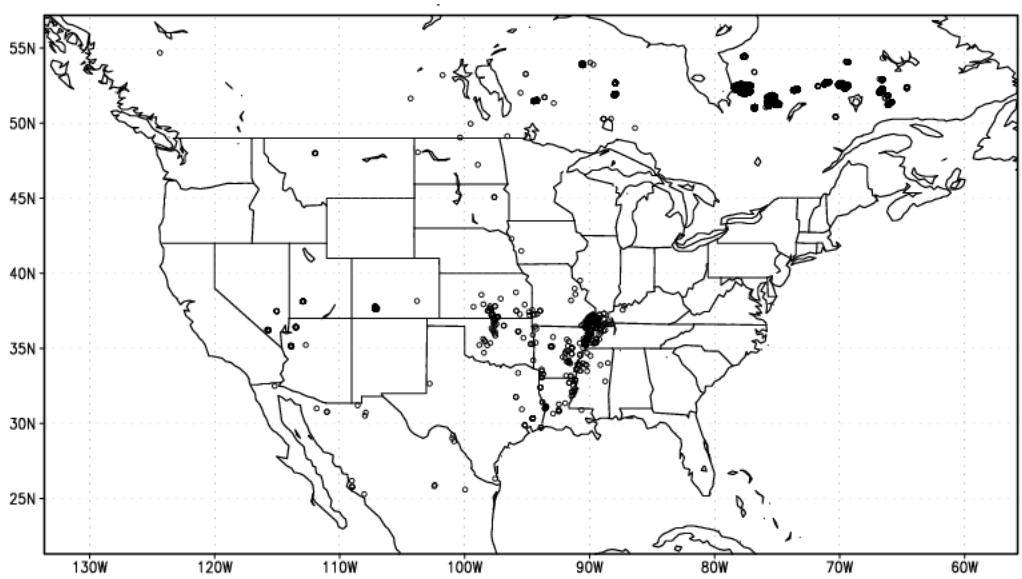

Figure 11b: fire hotspots in hmx.txt on July 03 2013 as daily composite.

Tables:

Table 1: observed and simulated CO (ppb) during NOAA SENEX

AGL (m)	SAMPLE SIZE	OBS	OBS_MAX	Mod_withfire	Mod_nofire	ΔCO
<500	166	128.93±38.51	319.55	108.70±21.37	107.16±20.34	1.54
500~1000	3565	146.19±44.39	1277.97	108.39±19.82	106.50±18.86	1.88
1000~1500	793	125.41±28.09	299.64	100.11±15.63	98.49±14.67	1.62
1500~2000	306	119.68±23.99	265.29	100.75±17.04	99.08±15.89	1.67
2000~2500	219	111.48±19.98	286.22	99.88±17.95	98.37±16.92	1.51
2500~3000	209	111.84±19.79	295.79	97.43±12.21	95.87±11.15	1.56
3000~3500	181	109.31±16.66	197.94	89.34±12.09	88.13±11.06	1.21
3500~4000	195	110.78±14.36	140.42	92.11±10.73	90.25±9.62	1.86
4000~5000	369	89.82±19.09	138.04	80.36±10.15	79.17±9.14	1.19
5000~6000	354	102.26±22.37	209.20	78.12±7.64	76.82±6.28	1.30
6000~7000	85	87.53±17.88	115.32	73.35±4.71	70.58±2.45	2.77

Table 2: identified fire signals from IMPROVE measurements during SENEX

Site	Date	Concentrations (ug m^{-3})						Ratio (Concentration/Average)						Ratio	
		EC	OC	K	SOIL	NO_3^-	SO_4^{2-}	EC	OC	K	SOIL	NO_3^-	SO_4^{2-}	BC/OC	K/BC
COHU	0621	0.28	2.10	0.05	0.22	0.13	2.61	1.4	1.46	1.42	0.39	0.84	1.28	0.1331	0.1933
MACA	0624	0.45	2.34	0.09	0.26	0.24	2.76	1.85	1.58	1.82	0.48	1.19	1.24	0.1929	0.1973
MACA	0703	0.33	2.32	0.08	0.16	0.29	2.11	1.35	1.57	1.73	0.29	1.43	0.94	0.1423	0.2554
BRIS	0703	0.24	0.98	0.21	0.31	0.11	2.63	1.49	1.28	2.79	0.13	0.35	1.36	0.2458	0.8851
GRSM	0621	0.25	1.56	0.05	0.24	0.13	2.52	1.36	1.45	1.24	0.49	0.99	1.42	0.1596	0.1979

Notes: (ratios for EC, OC and K > 1.2) **U** (ratio for SOIL < 1.0) **U** (ratios for NO_3^- and SO_4^{2-} < 1.5);

References:

Achtemeier, G. L., S. A. Goodrick, Y. Q. Liu, F. Garcia-Menendez, Y. T. Hu, and M. T. Odman. Modeling Smoke Plume-Rise and Dispersion from Southern United States Prescribed Burns with Daysmoke, *Atmosphere*, 2: 358-88. doi:10.3390/atmos2030358, 2011.

Aiken, A. C., B. de Foy, C. Wiedinmyer, P. F. DeCarlo, I. M. Ulbrich, M. N. Wehrli, S. Szidat, A. S. H. Prevot, J. Noda, L. Wacker, R. Volkamer, E. Fortner, J. Wang, A. Laskin, V. Shutthanandan, J. Zheng, R. Zhang, G. Paredes-Miranda, W. P. Arnott, L. T. Molina, G. Sosa, X. Querol, and J. L. Jimenez. Mexico city aerosol analysis during MILAGRO using high resolution aerosol mass spectrometry at the urban supersite (T0) - Part 2: Analysis of the biomass burning contribution and the non-fossil carbon fraction, *Atmospheric Chemistry and Physics*, 10: 5315-41. doi:10.5194/acp-10-5315-2010, 2010.

Alvarado, M. J., C. R. Lonsdale, R. J. Yokelson, S. K. Akagi, H. Coe, J. S. Craven, E. V. Fischer, G. R. McMeeking, J. H. Seinfeld, T. Soni, J. W. Taylor, D. R. Weise, and C. E. Wold. Investigating the links between ozone and organic aerosol chemistry in a biomass burning plume from a prescribed fire in California chaparral, *Atmospheric Chemistry and Physics*, 15: 6667-88. doi:10.5194/acp-15-6667-2015, 2015.

Baker, K. R., M. C. Woody, G. S. Tonnesen, W. Hutzell, H. O. T. Pye, M. R. Beaver, G. Pouliot, and T. Pierce. Contribution of regional-scale fire events to ozone and PM2.5 air quality estimated by photochemical modeling approaches, *Atmospheric Environment*, 140: 539-54. doi:10.1016/j.atmosenv.2016.06.032, 2016.

Carlton, A. G., P. V. Bhave, S. L. Napelenok, E. D. Edney, G. Sarwar, R. W. Pinder, G. A. Pouliot, and M. Houyoux. Model Representation of Secondary Organic Aerosol in CMAQv4.7, *Environmental Science & Technology*, 44: 8553-60. doi:10.1021/es100636q, 2010.

Chai, T., H. C. Kim, P. Lee, D. Tong, L. Pan, Y. Tang, J. Huang, J. McQueen, M. Tsidulko, and I. Stajner. Evaluation of the United States National Air Quality Forecast Capability experimental real-time predictions in 2010 using Air Quality System ozone and NO2 measurements, *Geoscientific Model Development*, 6: 1831-50. doi:10.5194/gmd-6-1831-2013, 2013.

Davis, A. Y., R. Ottmar, Y. Q. Liu, S. Goodrick, G. Achtemeier, B. Gullett, J. Aurell, W. Stevens, R. Greenwald, Y. T. Hu, A. Russell, J. K. Hiers, and M. T. Odman. Fire emission uncertainties and their effect on smoke dispersion predictions: a case study at Eglin Air Force Base, Florida, USA, *International Journal of Wildland Fire*, 24: 276-85. doi:10.1071/wf13071, 2015.

de Gouw, J. A., C. Warneke, D. D. Parrish, J. S. Holloway, M. Trainer, and F. C. Fehsenfeld. Emission sources and ocean uptake of acetonitrile (CH3CN) in the atmosphere, *Journal of Geophysical Research-Atmospheres*, 108. doi:10.1029/2002jd002897, 2003.

DeBell, L. J., R. W. Talbot, J. E. Dibb, J. W. Munger, E. V. Fischer, and S. E. Frolking. A major regional air pollution event in the northeastern United States caused by extensive forest fires in Quebec, Canada, *Journal of Geophysical Research-Atmospheres*, 109. doi:10.1029/2004jd004840, 2004.

Delfino, R. J., S. Brummel, J. Wu, H. Stern, B. Ostro, M. Lipsett, A. Winer, D. H. Street, L. Zhang, T. Tjoa, and D. L. Gillen. The relationship of respiratory and cardiovascular hospital admissions to the southern California wildfires of 2003, *Occupational and Environmental Medicine*, 66: 189-97. doi:10.1136/oem.2008.041376, 2009.

Draxler, R. R., and G. D. Hess. An overview of the HYSPLIT_4 modelling system for trajectories, dispersion and deposition, *Australian Meteorological Magazine*, 47: 295-308. 1998.

Dreessen, J., J. Sullivan, and R. Delgado. Observations and impacts of transported Canadian wildfire smoke on ozone and aerosol air quality in the Maryland region on June 9-12, 2015, *Journal of the Air & Waste Management Association*, 66: 842-62. doi:10.1080/10962247.2016.1161674, 2016.

Drury, S. A., N. Larkin, T. T. Strand, S. M. Huang, S. J. Strenfel, E. M. Banwell, T. E. O'Brien, and S. M. Raffuse. INTERCOMPARISON OF FIRE SIZE, FUEL LOADING, FUEL CONSUMPTION, AND SMOKE EMISSIONS ESTIMATES ON THE 2006 TRIPOD FIRE,WASHINGTON, USA, *Fire Ecology*, 10: 56-83. doi:10.4996/fireecology.1001056, 2014.

Eatough, D. J., D. A. Eatough, L. Lewis, and E. A. Lewis. Fine particulate chemical composition and light extinction at Canyonlands National Park using organic particulate material concentrations obtained with a multisystem, multichannel diffusion denuder sampler, *Journal of Geophysical Research-Atmospheres*, 101: 19515-31. doi:10.1029/95jd01385, 1996.

Erbrink, H. J. PLUME RISE IN DIFFERENT ATMOSPHERES - A PRACTICAL SCHEME AND SOME COMPARISONS WITH LIDAR MEASUREMENTS, *Atmospheric Environment*, 28: 3625-36. doi:10.1016/1352-2310(94)00197-s, 1994.

Giglio, L., J. Descloitres, C. O. Justice, and Y. J. Kaufman. An enhanced contextual fire detection algorithm for MODIS, *Remote Sensing of Environment*, 87: 273-82. doi:10.1016/s0034-4257(03)00184-6, 2003.

Hamm, S., and P. Warneck. THE INTERHEMISPHERIC DISTRIBUTION AND THE BUDGET OF ACETONITRILE IN THE TROPOSPHERE, *Journal of Geophysical Research-Atmospheres*, 95: 20593-606. doi:10.1029/JD095iD12p20593, 1990.

Hardy, C. C., and C. E. Hardy. Fire danger rating in the United States of America: an evolution since 1916, *International Journal of Wildland Fire*, 16: 217-31. doi:10.1071/wf06076, 2007.

Herron-Thorpe, F. L., G. H. Mount, L. K. Emmons, B. K. Lamb, D. A. Jaffe, N. L. Wigder, S. H. Chung, R. Zhang, M. D. Woelfle, and J. K. Vaughan. Air quality simulations of wildfires in the Pacific Northwest evaluated with surface and satellite observations during the summers of 2007 and 2008, *Atmospheric Chemistry and Physics*, 14: 12533-51. doi:10.5194/acp-14-12533-2014, 2014.

Holzinger, R., C. Warneke, A. Hansel, A. Jordan, W. Lindinger, D. H. Scharffe, G. Schade, and P. J. Crutzen. Biomass burning as a source of formaldehyde, acetaldehyde, methanol, acetone, acetonitrile, and hydrogen cyanide, *Geophysical Research Letters*, 26: 1161-64. doi:10.1029/1999gl900156, 1999.

Hu, X. F., C. Yu, D. Tian, M. Ruminski, K. Robertson, L. A. Waller, and Y. Liu. Comparison of the Hazard Mapping System (HMS) fire product to ground-based fire records in Georgia, USA, *Journal of Geophysical Research-Atmospheres*, 121: 2901-10. doi:10.1002/2015jd024448, 2016.

Huang, J., J. McQueen, J. Wilczak, I. Djalalova, I. Stajner, P. Shafran, D. Allured, P. Lee, L. Pan, D. Tong, H. Huang, G. DiMego, S. Upadhayay, and L. Monache. Improving NOAA NAQFC PM2.5 predictions with a bias correction approach, *Wea. Forecasting*. doi:10.1175/WAF-D-16-0118.1, 2017.

Jaffe, D. A., N. Wigder, N. Downey, G. Pfister, A. Boynard, and S. B. Reid. Impact of Wildfires on Ozone Exceptional Events in the Western US, *Environmental Science & Technology*, 47: 11065-72. doi:10.1021/es402164f, 2013.

Johnston, F. H., S. B. Henderson, Y. Chen, J. T. Randerson, M. Marlier, R. S. DeFries, P. Kinney, Dmjs Bowman, and M. Brauer. Estimated Global Mortality Attributable to Smoke from Landscape Fires, *Environmental Health Perspectives*, 120: 695-701. doi:10.1289/ehp.1104422, 2012.

Justice, C. O., L. Giglio, S. Korontzi, J. Owens, J. T. Morisette, D. Roy, J. Descloitres, S. Alleaume, F. Petitcolin, and Y. Kaufman. The MODIS fire products, *Remote Sensing of Environment*, 83: 244-62. doi:10.1016/s0034-4257(02)00076-7, 2002.

Knorr, W., V. Lehsten, and A. Arneth. Determinants and predictability of global wildfire emissions, *Atmospheric Chemistry and Physics*, 12: 6845-61. doi:10.5194/acp-12-6845-2012, 2012.

Larkin, N. K., S. M. O'Neill, R. Solomon, S. Raffuse, T. Strand, D. C. Sullivan, C. Krull, M. Rorig, J. L. Peterson, and S. A. Ferguson. The BlueSky smoke modeling framework, *International Journal of Wildland Fire*, 18: 906-20. doi:10.1071/wf07086, 2009.

Lee, Pius, Jeffery McQueen, Ivanka Stajner, Jianping Huang, Li Pan, Daniel Tong, Hyuncheol Kim, Youhua Tang, Shobha Kondragunta, and Mark Ruminski. NAQFC developmental forecast guidance for fine particulate matter (PM2. 5), *Weather and Forecasting*, 32: 343-60. doi:10.1175/waf-d-15-0163.1, 2017.

Li, Z., S. Nadon, and J. Cihlar. Satellite-based detection of Canadian boreal forest fires: development and application of the algorithm, *International Journal of Remote Sensing*, 21: 3057-69. doi:10.1080/01431160050144956, 2000.

Malm, W. C., B. A. Schichtel, M. L. Pitchford, L. L. Ashbaugh, and R. A. Eldred. Spatial and monthly trends in speciated fine particle concentration in the United States, *Journal of Geophysical Research-Atmospheres*, 109. doi:10.1029/2003jd003739, 2004.

Neuman, J. A., M. Trainer, S. S. Brown, K. E. Min, J. B. Nowak, D. D. Parrish, J. Peischl, I. B. Pollack, J. M. Roberts, T. B. Ryerson, and P. R. Veres. HONO emission and production determined from airborne measurements over the Southeast US, *Journal of Geophysical Research-Atmospheres*, 121: 9237-50. doi:10.1002/2016jd025197, 2016.

Pan, L., D. Tong, P. Lee, H. C. Kim, and T. F. Chai. Assessment of NOx and O-3 forecasting performances in the US National Air Quality Forecasting Capability before and after the 2012 major emissions updates, *Atmospheric Environment*, 95: 610-19. doi:10.1016/j.atmosenv.2014.06.020, 2014.

Pavlovic, R., J. Chen, K. Anderson, M. D. Moran, P. A. Beaulieu, D. Davignon, and S. Cousineau. The FireWork air quality forecast system with near-real-time biomass burning emissions: Recent developments and evaluation of performance for the 2015 North American wildfire season, *Journal of the Air & Waste Management Association*, 66: 819-41. doi:10.1080/10962247.2016.1158214, 2016.

Prados, A. I., S. Kondragunta, P. Ciren, and K. R. Knapp. GOES Aerosol/Smoke product (GASP) over North America: Comparisons to AERONET and MODIS observations, *Journal of Geophysical Research-Atmospheres*, 112. doi:10.1029/2006jd007968, 2007.

Prins, E. M., and W. P. Menzel. GEOSTATIONARY SATELLITE DETECTION OF BIOMASS BURNING IN SOUTH-AMERICA, *International Journal of Remote Sensing*, 13: 2783-99. 1992.

Rappold, A. G., S. L. Stone, W. E. Cascio, L. M. Neas, V. J. Kilaru, M. S. Carraway, J. J. Szykman, A. Ising, W. E. Cleve, J. T. Meredith, H. Vaughan-Batten, L. Deyneka, and R. B. Devlin. Peat Bog Wildfire Smoke Exposure in Rural North Carolina Is Associated with Cardiopulmonary Emergency Department Visits Assessed through Syndromic Surveillance, *Environmental Health Perspectives*, 119: 1415-20. doi:10.1289/ehp.1003206, 2011.

Reid, J. S., R. Koppmann, T. F. Eck, and D. P. Eleuterio. A review of biomass burning emissions part II: intensive physical properties of biomass burning particles, *Atmospheric Chemistry and Physics*, 5: 799-825. 2005.

Rolph, G. D., R. R. Draxler, A. F. Stein, A. Taylor, M. G. Ruminski, S. Kondragunta, J. Zeng, H. C. Huang, G. Manikin, J. T. McQueen, and P. M. Davidson. Description and Verification of the NOAA Smoke Forecasting System: The 2007 Fire Season, *Weather and Forecasting*, 24: 361-78. doi:10.1175/2008waf2222165.1, 2009.

Ruminski, M., and S. Kondragunta. Monitoring fire and smoke emissions with the hazard mapping system - art. no. 64120B. in F. Kogan, S. Habib, V. S. Hegde and M. Matsuoka (eds.), *Disaster Forewarning Diagnostic Methods and Management*. 2006.

Ruminski, M., J. Simko, J. Kibler, S. Kondragunta, R. Draxler, P. Davidson, and P. Li. Use of multiple satellite sensors in NOAA's operational near real-time fire and smoke detection and characterization program. in W. M. Hao (ed.), *Remote Sensing of Fire: Science and Application*. 2008.

Saide, P. E., D. A. Peterson, A. da Silva, B. Anderson, L. D. Ziemba, G. Diskin, G. Sachse, J. Hair, C. Butler, M. Fenn, J. L. Jimenez, P. Campuzano-Jost, A. E. Perring, J. P. Schwarz, M. Z. Markovic, P. Russell,

J. Redemann, Y. Shinozuka, D. G. Streets, F. Yan, J. Dibb, R. Yokelson, O. B. Toon, E. Hyer, and G. R. Carmichael. Revealing important nocturnal and day-to-day variations in fire smoke emissions through a multiplatform inversion, *Geophysical Research Letters*, 42: 3609-18. doi:10.1002/2015gl063737, 2015.

Sandberg, D.V., and J. Peterson. A source strength model for prescribed fires in coniferous logging slash, *1984 annual meeting, Air Pollution Control Association, Northwest Section. 14p*. 1984.

Sapkota, A., J. M. Symons, J. Kleissl, L. Wang, M. B. Parlange, J. Ondov, P. N. Breysse, G. B. Diette, P. A. Eggleston, and T. J. Buckley. Impact of the 2002 Canadian forest fires on particulate matter air quality in Baltimore City, *Environmental Science & Technology*, 39: 24-32. doi:10.1021/es035311z, 2005.

Schroeder, W., M. Ruminski, I. Csiszar, L. Giglio, E. Prins, C. Schmidt, and J. Morisette. Validation analyses of an operational fire monitoring product: The Hazard Mapping System, *International Journal of Remote Sensing*, 29: 6059-66. doi:10.1080/01431160802235845, 2008.

Singh, H. B., C. Cai, A. Kaduwela, A. Weinheimer, and A. Wisthaler. Interactions of fire emissions and urban pollution over California: Ozone formation and air quality simulations, *Atmospheric Environment*, 56: 45-51. doi:10.1016/j.atmosenv.2012.03.046, 2012.

Singh, H. B., L. Salas, D. Herlth, R. Kolyer, E. Czech, W. Viezee, Q. Li, D. J. Jacob, D. Blake, G. Sachse, C. N. Harward, H. Fuelberg, C. M. Kiley, Y. Zhao, and Y. Kondo. In situ measurements of HCN and CH3CN over the Pacific Ocean: Sources, sinks, and budgets, *Journal of Geophysical Research-Atmospheres*, 108. doi:10.1029/2002jd003006, 2003.

Sofiev, M., T. Ermakova, and R. Vankevich. Evaluation of the smoke-injection height from wild-land fires using remote-sensing data, *Atmospheric Chemistry and Physics*, 12: 1995-2006. doi:10.5194/acp-12-1995-2012, 2012.

Strand, T. M., N. Larkin, K. J. Craig, S. Raffuse, D. Sullivan, R. Solomon, M. Rorig, N. Wheeler, and D. Pryden. Analyses of BlueSky Gateway PM2.5 predictions during the 2007 southern and 2008 northern California fires, *Journal of Geophysical Research-Atmospheres*, 117. doi:10.1029/2012jd017627, 2012.

Urbanski, S., V. Kovalev, A. Petkov, A. Scalise, C. Wold, and W. M. Hao. Validation of smoke plume rise models using ground-based lidar. in C. M. U. Neale and A. Maltese (eds.), *Remote Sensing for Agriculture, Ecosystems, and Hydrology Xvi*. 2014.

Warneke, C., M. Trainer, J. A. de Gouw, D. D. Parrish, D. W. Fahey, A. R. Ravishankara, A. M. Middlebrook, C. A. Brock, J. M. Roberts, S. S. Brown, J. A. Neuman, B. M. Lerner, D. Lack, D. Law, G. Hubler, I. Pollack, S. Sjostedt, T. B. Ryerson, J. B. Gilman, J. Liao, J. Holloway, J. Peischl, J. B. Nowak, K. C. Aikin, K. E. Min, R. A. Washenfelder, M. G. Graus, M. Richardson, M. Z. Markovic, N. L. Wagner, A. Welti, P. R. Veres, P. Edwards, J. P. Schwarz, T. Gordon, W. P. Dube, S. A. McKeen, J. Brioude, R. Ahmadov, A. Bougiatioti, J. J. Lin, A. Nenes, G. M. Wolfe, T. F. Hanisco, B. H. Lee, F. D. Lopez-Hilfiker, J. A. Thornton, F. N. Keutsch, J. Kaiser, J. Q. Mao, and C. D. Hatch. Instrumentation and measurement strategy for the NOAA SENEX aircraft campaign as part of the Southeast Atmosphere Study 2013, *Atmospheric Measurement Techniques*, 9: 3063-93. doi:10.5194/amt-9-3063-2016, 2016.

Wiedinmyer, C., S. K. Akagi, R. J. Yokelson, L. K. Emmons, J. A. Al-Saadi, J. J. Orlando, and A. J. Soja. The Fire INventory from NCAR (FINN): a high resolution global model to estimate the emissions from open burning, *Geoscientific Model Development*, 4: 625-41. doi:10.5194/gmd-4-625-2011, 2011.

Wiedinmyer, C., B. Quayle, C. Geron, A. Belote, D. McKenzie, X. Y. Zhang, S. O'Neill, and K. K. Wynne. Estimating emissions from fires in North America for air quality modeling, *Atmospheric Environment*, 40: 3419-32. doi:10.1016/j.atmosenv.2006.02.010, 2006.

Wotawa, G., and M. Trainer. The influence of Canadian forest fires on pollutant concentrations in the United States, *Science*, 288: 324-28. doi:10.1126/science.288.5464.324, 2000.

Xu, L., A. M. Middlebrook, J. Liao, J. A. de Gouw, H. Y. Guo, R. J. Weber, A. Nenes, F. D. Lopez-Hilfiker, B. H. Lee, J. A. Thornton, C. A. Brock, J. A. Neuman, J. B. Nowak, I. B. Pollack, A. Welti, M. Graus, C. Warneke, and N. L. Ng. Enhanced formation of isoprene-derived organic aerosol in sulfur-rich power plant plumes during Southeast Nexus, *Journal of Geophysical Research-Atmospheres*, 121: 11137-53. doi:10.1002/2016jd025156, 2016.

Yarwood, G., S. Rao, M. Yocke, and G. Whitten. Updates to the Carbon Bond Chemical Mechanism: CB05, *Technical Report RT-0400675 ENVIRON International Corporation Novato, CA, USA*. 2005.

Zhang, X. Y., S. Kondragunta, and B. Quayle. Estimation of Biomass Burned Areas Using Multiple-Satellite-Observed Active Fires, *Ieee Transactions on Geoscience and Remote Sensing*, 49: 4469-82. doi:10.1109/tgrs.2011.2149535, 2011.